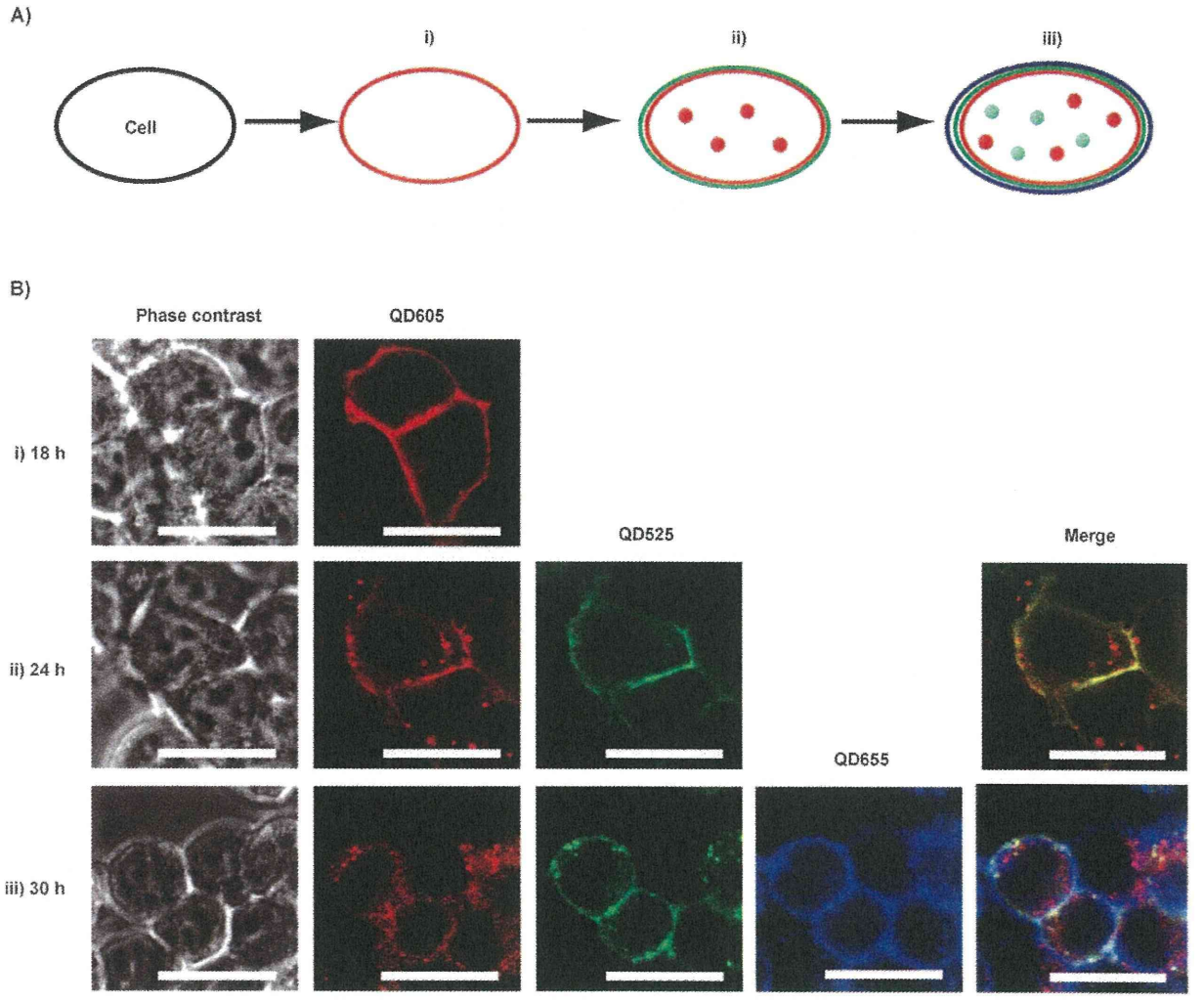

Figure 3. A) Schematic representation of the pulse-chase labeling of BL-EGFR labeled with three QDs. B) Fluorescence images of QDs-labeled BL-EGFR i) 18, ii) 24, and iii) 30 h after transfection. Scale bar = 20 μm.

chase imaging of EGFR was successful with feasible experimental setups with BL-tag and QDs; these experiments are not successful with use of fluorescent proteins. Imaging was successful with a single excitation laser and a single expressed protein, so the photochemical characteristics of the QDs were well suited for monitoring the timing of protein expression.

In conclusion, we have developed a novel biotinylation probe, BHA, and have demonstrated its application in fluorescence imaging of POIs on living cell surfaces. EGFR fused with BL-tag was selectively biotinylated and successively labeled with various colors of QD through streptavidin–biotin binding. Our previous labeling method, based on small-molecular fluorescent probes, was modified for use with BHA. Because QDs are more resistant to photobleaching than the fluorescein-based probe, this technology should be useful for experiments that require strong excitation. This method was also applicable to time-lapse fluorescence imaging of EGFR internalization. Moreover, we successfully labeled proteins at different expression times on cell surfaces with three different colors of QD. This pulse-chase labeling is a powerful method for studying dynamic cellular processes, such as biological structure formation. Furthermore, if near-infrared-fluorescent QDs are used, this method can be applied to in vivo imaging studies. These versatile properties of the biotin-labeling technology should allow studies of various protein functions and lead to the development of new drugs or therapeutic approaches.

Experimental Section

Detailed experimental procedures for the synthesis and characterization of all compounds, as well as a detailed description of all experiments, are given in the Supporting Information.

Acknowledgements

This work was supported in part by a Grant-in-Aid for Scientific Research from the Ministry of Education, Culture, Sports, Science

and Technology (MEXT) of Japan, by a Grant-in-Aid from the Ministry of Health, Labor, and Welfare (MHLW) of Japan, by the Funding Program for World-Leading Innovative R&D on Science and Technology from the Japan Society for the Promotion of Science (JSPS), and by the Japan Science and Technology Agency Core Research for Evolutional Science and Technology (JST CREST).

Keywords: biotinylation · epidermal growth factor receptor · fluorescence · mutant beta-lactamase · quantum dots

[1] X. Michalet, F. F. Pinaud, L. A. Bentolia, J. M. Tsay, S. Doose, J. J. Li, G. Sundaresan, A. M. Wu, S. S. Gambhir, S. Weiss, *Science* **2005**, *307*, 538–544.

[2] M. Howarth, K. Takao, Y. Hayashi, A. Y. Ting, *Proc. Natl. Acad. Sci. USA* **2005**, *102*, 7583–7588.

[3] M. K. So, H. Yao, J. Rao, *Biochem. Biophys. Res. Commun.* **2008**, *374*, 419–423.

[4] a) G. V. Los, L. P. Encell, M. G. McDougall, D. D. Hartzell, N. Karassina, C. Zimprich, M. G. Wood, R. Learish, R. F. Ohana, M. Urh, D. Simpson, J. Mendez, K. Zimmerman, P. Otto, G. Vidugiris, J. Zhu, A. Darzins, D. H. Klaubert, R. F. Bulleit, K. V. Wood, *ACS Chem. Biol.* **2008**, *3*, 373–382; b) A. Keppler, S. Gendreizig, T. Gronemeyer, H. Pick, H. Vogel, K. Johnsson, *Nat. Biotechnol.* **2002**, *21*, 86–89; c) S. S. Gallagher, J. E. Sable, M. P. Sheetz, V. W. Cornish, *ACS Chem. Biol.* **2009**, *4*, 547–556.

[5] a) B. A. Griffin, S. R. Adams, R. Y. Tsien, *Science* **1998**, *281*, 269–272; b) A. Ojida, K. Honda, D. Shinmi, S. Kiyonaka, Y. Mori, I. Hamachi, *J. Am. Chem. Soc.* **2006**, *128*, 10452–10459; c) C. T. Hauser, R. Y. Tsien, *Proc. Natl. Acad. Sci. USA* **2007**, *104*, 3693–3697.

[6] a) I. Chen, M. Howarth, W. Lin, A. Y. Ting, *Nat. Methods* **2005**, *2*, 99–104; b) N. George, H. Pick, H. Vogel, N. Johnsson, K. Johnsson, *J. Am. Chem. Soc.* **2004**, *126*, 8896–8897.

[7] a) S. Mizukami, S. Watanabe, Y. Hori, K. Kikuchi, *J. Am. Chem. Soc.* **2009**, *131*, 5016–5017; b) S. Watanabe, S. Mizukami, Y. Hori, K. Kikuchi, *Bioconjugate Chem.* **2010**, *21*, 2320–2326.

[8] K. K. Sadhu, S. Mizukami, S. Watanabe, K. Kikuchi, *Chem. Commun.* **2010**, *46*, 7403–7405.

[9] a) Q. Wang, G. Villeneuve, Z. Wang, *EMBO Rep.* **2005**, *6*, 942–948; b) D. L. Wheeler, E. F. Dunn, P. M. Harari, *Nat. Rev. Clin. Oncol.* **2010**, *7*, 493–507.

[10] R. E. Carter, A. Sorkin, *J. Biol. Chem.* **1998**, *273*, 35000–35007.

[11] a) R. Brock, R. B. Hamelers, T. M. Jovin, *Cytometry* **1999**, *35*, 353–362; b) D. S. Lidke, P. Nagy, R. Heintzmann, D. J. A. Jovin, J. N. Post, H. E. Grecco, E. A. J. Erijman, T. M. Jovin, *Nat. Biotechnol.* **2004**, *22*, 198–203.

[12] a) Q. Yuan, E. Lee, W. A. Yeudall, H. Yang, *Oral Oncol.* **2010**, *46*, 698–704; b) J. Lee, Y. Choi, K. Kim, S. Hong, H. Y. Park, T. Lee, G. J. Cheon, R. Song, *Bioconjugate Chem.* **2010**, *21*, 940–946; c) H. Xu, P. K. Eck, K. E. Baidoo, P. L. Choyke, M. W. Brechbiel, *Bioorg. Med. Chem.* **2009**, *17*, 5176–5181.

Received: January 12, 2011
Published online on March 18, 2011

DOI: 10.1002/cbic.201100137

Switching Modulation for Protein Labeling with Activatable Fluorescent Probes

Kalyan K. Sadhu,[a] Shin Mizukami,[a, b] Yuichiro Hori,[a] and Kazuya Kikuchi*[a, b]

Introduction

Real-time monitoring of protein dynamics and communicating mechanisms within living cells, protein position, and interactions with other proteins can be rationalized by protein labeling studies with fluorescent molecules. This detailed analysis at the subcellular level might provide a comprehensive understanding of the multifaceted biochemical and structural modifications associated with cell activities and function.[1,2]

For several decades, fluorescent proteins (FPs) have been the most accepted method for protein labeling studies. The first applied fluorescent protein was green fluorescent protein (GFP).[3–5] The amino acid residues at positions 65–67 (Ser-Tyr-Gly) of the 238 amino acids readily form the fluorescent chromophore.[6–9] The extensive use of GFP probes was piloted by simultaneous progress on reporters and biomolecular imaging techniques to locate fusion-protein expression, in real time and real space, in single living cells.[10–14] GFP was used as a probe to study several functions, such as gene expression, protein localization, dynamics, and protein–protein interaction. GFP was also used for altering pH-based sensors, and for the measurement of Ca^{2+} concentration in living cells.[15] With the improvements in the understanding of cell signaling process, scientists are now concentrating on labeling to elucidate the sophisticated properties of proteins.

In spite of several fruitful applications, use of these GFP probes is constrained by certain limitations including their large size[16,17] and the limited variety of their colors. To overcome the limited spectral variety of GFP, a recent outcome has been the improved red FP variants.[18]

To overcome the limitations of FPs, some alternate approaches for live-cell labeling have been developed in the recent past.[19,20] Bright and photostable small fluorophores can be superior to their fluorescent protein counterparts and overcome the shortcomings of an intrinsic protein because of robust modification for target processes and nonfluorogenicity.[21] To incorporate a small molecule into a protein sequence researchers have used the binding affinity of proteins to a probe. In this method, the most-used techniques involve fusion of the protein of interest (POI) to a protein or peptide tag that is competent for binding to the small molecular probe. Antibody tags have been fused to specific signal sequences for targeting various fluorophore conjugates to label specific intracellular targets in living cells.[22] Dihydrofolate reductase (DHFR)[20] and the Phe36Val mutant[23–27] of FK506-binding protein-12 (FKBP12) bind to the small-molecule ligands methotrexate and to a synthetic ligand, respectively, by noncovalent interactions.

The site-specific nature of GFP reporters results from their genetic fusion with the POI. But the fluorogenic property of the tag is absent in case of FPs. The time of fluorescence intensity cannot be controlled in GFP, whereas fluorogenicity can be controlled in the case of small molecular probes. This fluorogenicity is extremely important as it renders rigorous washing (to remove excess small molecular probe) unnecessary. The paucity of site-specific protein labeling methodologies is the major hurdle for the exploitation of small molecular probes in protein labeling. The chemoselectivity of a small-molecule probe towards a unique functional group of a single protein (among the thousands other competing proteins) poses an enormous chemical problem. Among the several small molecular probes for protein labeling there are limited examples of fluorogenic probes, and the fluorescence states of the probes alter only after the protein labeling process. To the best of our knowledge, until December 2010 there was only one review article, and it covers only one type of "turn-on" protein-labeling methodology.[28] We focus here on the research associated with turn-on-type fluorogenic small probes for protein labeling. A large number of fluorogenic small molecular probes with low specificity have been applied for protein labeling. But site-specific turn-on-type small probes have been studied by us and by some other groups in recent years. Herein, we summarize only the activatable fluoroscent probes used for protein labeling in living systems. We avoid discussion of successful labeling in vitro (i.e., without translation).

2. FlAsH and Modification of FlAsH

2.1. FlAsH

During the end of last century Tsien's group developed a "turn-on" method for specifically labeling proteins in living cells. As^{III} compounds can form covalent linkages with closely

[a] Dr. K. K. Sadhu, Dr. S. Mizukami, Dr. Y. Hori, Prof. Dr. K. Kikuchi
Division of Advanced Science and Biotechnology
Graduate School of Engineering
Osaka University
2–1 Yamadaoka, Suita, Osaka 565-0871 (Japan)
Fax: (+81) 6-6879-7875
E-mail: kkikuchi@mls.eng.osaka-u.ac.jp

[b] Dr. S. Mizukami, Prof. Dr. K. Kikuchi
Immunology Frontier Research Center, Osaka University
3–1 Yamadaoka, Suita, Osaka 565-0871 (Japan)

spaced paired cysteine-thiol groups in proteins. Based on this interaction, an interacting pair has been developed that consists of a small peptide tag with tetracysteine (TC) motif and a biarsenical probe.[29,30] In the TC part, two cysteine pairs are separated by a spacer of another two different amino acids (CCXXCC), and this motif binds to organo-arsenical compounds under reducing conditions. This successful strategy was named "fluorescein arsenical hairpin binder" (FlAsH); for this, a fluorescein fluorophore has thioarsolane substitutions at the 4′ and 5′ positions (Scheme 1). The covalent interactions between two

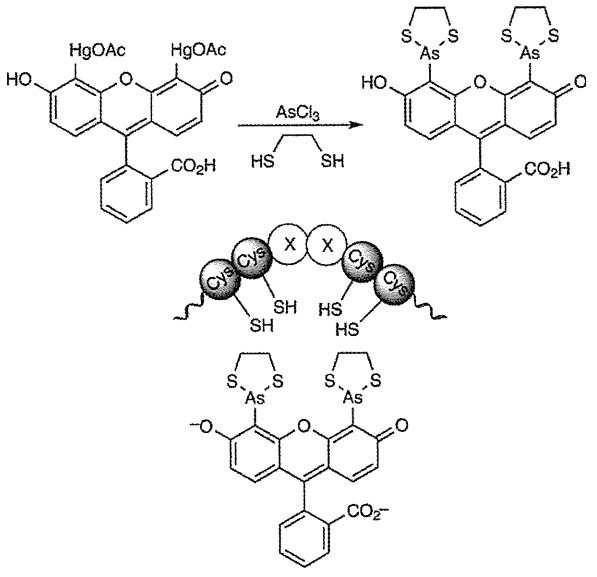

Scheme 1. A) Synthesis of FlAsH-EDT$_2$ and B) reaction with tetracysteine-containing peptide or protein domain.

cysteine pairs and the biarsenical part of FlAsH have small effective dissociation constants.[31] A recent report suggested that the binding affinity between a FlAsH reagent and the TC motif is stable against high pressure, high field strength, high temperature, and ultrasound.[32] This strong covalent interaction reduces the toxic effect of arsenic on the function of other proteins.

The genetic fusion of the small peptide TC tag with the POI allows labeling of the specific fusion protein in living cells on incubation with FlAsH.[29] The free biarsenal moiety is in a quenched state until it covalently links with the TC motif. The covalent interaction results in a significant increase of fluorescence intensity.[29] For protein labeling studies mutant calmodulin was used, in which four residues at the N-terminal of a helix were replaced with cysteines. This was expressed in the cytosol and nuclei of HeLa cells, and became brightly fluorescent when treated with FlAsH-EDT$_2$ (Figure 1). A control experiment with nontransfected cells in a different dish showed background labeling. In the earlier stages it was presumed that a short α-helix at the peptide end would provide an optimal binding environment for the thioarsenal moiety.[29] However, extensive exploration of several peptide motifs with different spacers in the TC part has revealed that the introduction of glycine and proline in the amino acid sequence yields a significant contribution towards binding affinity between FlAsH and the TC motif.[31] This work also revealed that the preferred conformation of the peptide sequence is a hairpin rather than an α-helix. Kinesin tagged with a TC-containing helix bound specifically to FlAsH resin and was eluted in a fully active form.[33] A recent modification that used two new peptide sequences (FLNCCPGCCMEP and HWRCCPGCCKTF) revealed a higher affinity for biarsenical dyes— and with higher quantum yield.[34] The enhancement was found to be at least 20 times superior to the previous standard motif (CCPGCC).

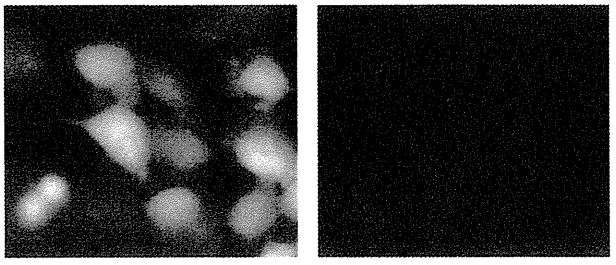

Figure 1. FlAsH labeling of a tetracysteine motif inserted within a protein. Left: Fluorescence images (excitation 480 ± 15 nm, emission 535 ± 12.5 nm) of HeLa cells transiently transfected with a gene for Cys-calmodulin. Right: Nontransfected HeLa cells labeled and imaged under identical conditions. Reprinted with permission from ref. [29]. Copyright 1998, the American Association for the Advancement of Science.

FlAsH-TC motif binding affinity has been employed with synaptotagmin I (SytI4C).[35] Neuronally expressed SytI4C rescued the *sytI* null mutation, as was visualized after FlAsH labeling. Efficient fluorophore-assisted light inactivation (FlAsH-FALI) of SytI was monitored by illumination (488 nm) of FlAsH bound to SytI4C. The inactivation of SytI was proportional to the time of illumination, and followed first-order kinetics.

Lipid rafts are the specialized membranes used for the assembly and budding of Ebola virus particles. To determine the raft localization of matrix protein VP40 and its mutants in intact cells, TC-VP40-transfected 293T cells were analyzed for VP40 localization after staining with FlAsH.[36] VP40 plays a critical role in this assembly process and it was mainly located at the plasma membrane. With Alexa 594 CTB co-staining to visualize the rafts, the membrane-bound VP40 was found to co-localize with rafts.

The TC/FlAsH technique has been proved more useful than yellow fluorescence protein (YFP) for the activation of G protein-coupled receptors in living cells. Fluorescence resonance energy transfer (FRET) between cyan fluorescence protein (CFP) and YFP was employed for monitoring the activation of human adenosine A_{2A} receptors. The CFP/FlAsH-TC system shows a fivefold enhancement compared to FRET signals, yet with similar kinetics and normal downstream signaling.[37]

Prion diseases are characterized by the disease associated prion protein form (PrP^{Sc}), which is created from the misfolding of the host-encoded cellular prion protein (PrP^{C}). PrP^{C} adopts a predominantly α-helix-rich conformation (α-PrP), whereas PrP^{Sc} has a protease-resistant form (β-sheet rich). FlAsH-induced

changes in fluorescence intensities (derived from TC-tagged recombinant PrP) were different between α- and β-PrP. The fluorescence enhancement after the labeling process for PrP in the α-helical form was much lower when compared to the same labeling experiment for β-PrP.[38] A recent technique, "Instant with DTT, EDT, and Low" (IDEAL) temperature labeling, has been developed for the rapid and specific FlAsH labeling of TC-tagged cell surface proteins; PrP and amyloid precursor protein (APP) were used as models.[39]

The FlAsH/TC labeling system has also been used to fluorescently tag specific effectors in Gram-negative pathogenic bacteria such as *Salmonella* to observe real-time secretion of bacterial effector proteins in a mammalian host cell.[40]

2.2. Modification of FlAsH

In spite of the drawbacks of the FlAsH technique, such as nonspecificity, there are noteworthy reports of FlAsH applications[29–56] that emphasize the versatility and breadth of potential applications. Modification of the FlAsH methodology overcame the color limitation of GFP labeling by introducing two additional biarsenical dyes: the resorufin-derived red fluorescent dye ReAsH (Scheme 2A) and the blue fluorescing 3,6-dihydroxyxanthone derivatized biarsenical ChoXAsH (Scheme 2B).[30] FlAsH is more commonly used for biomolecular imaging, while ReAsH induces phenotypic changes under certain conditions, and has lower photostability.

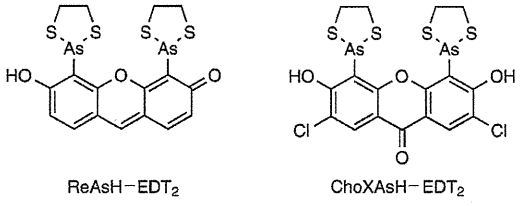

Scheme 2. Structures of A) ReAsH-EDT_2 and B) ChoXAsH-EDT_2.

This technology has also been applied with the modification of an environmentally sensitive biarsenical dye based on nile red to monitor calcium-induced protein conformation changes in calmodulin.[41]

GFP has helped to monitor the secretion of cytochrome *c* from mitochondria. But due to fusion, the release during apoptosis might not reflect the actual amount of cytochrome *c* released. To resolve the problem TC was fused to cytochrome *c*, and this was labeled in living cells by exposure to FlAsH or ReAsH. Cytochrome *c*-4CYS was expressed in HeLa cells. By comparison with the mitochondrial markers Mitotracker Green, the efficient localization in the mitochondria of these cells by FlAsH and ReAsH was monitored in an imaging study.[42]

The sequence CCKACC yields the same brightness as that of the classical CCPGCC sequence upon multiuse affinity probe (MAP) binding, but the rates and affinities of association towards ReAsH-EDT_2 or FLAsH-EDT_2 are different. This allows orthogonal labeling of these peptide sequences by ReAsH-EDT_2 or FLAsH-EDT_2 in complex cellular lystates with spectroscopically distinct MAPs.[43] Specific labeling by ReAsH-EDT_2 was observed for the PG-tag in the *E. coli* RNA polymerase α-subunit in cellular lysate, whereas FlAsH-EDT_2 labeled a KA-tag sequence in the β-subunit. The development of a sequential labeling method for two short peptide linkages, CCPGCC and FLNCCPGCCMEP, afforded site-specific protein labeling with FlAsH and ReAsH, respectively.[44] Cell imaging studies that involved colocalization and FRET were performed with the cell surface receptor for parathyroid hormone and its cytosolic binding protein, β-arrestin2.

A simple two-step route has been developed for the membrane-permeant fluorogenic biarsenicals FlAsH-EDT_2 and ReAsH-EDT_2.[45] This was used to study the intracellular localization of proteins and functional interactions in FRET experiments.[46]

An efficient technique has been developed for introducing FlAsH-EDT_2 into *Dictyostelium*; in this, a modified filamin gene was transfected into cells. The fluorescence intensity within the cells increased with time after addition of either FlAsH-EDT_2 or ReAsH-EDT_2, and reached a maximum after 3 h of incubation.[47] This tagging system has also been demonstrated in live budding yeast cells by standard electroporation. This reduces the labeling time drastically without compromising labeling efficiency.[48]

Human immunodeficiency virus type 1 (HIV-1) Gag is the primary structural protein of the virus and is essential for particle formation. A TC motif was added to the C terminus of Gag and specifically labeled by FlAsH and ReAsH to dynamically observe HIV-1 Gag within live HeLa cells by deconvolution fluorescence microscopy.[49] Gag-TC was localized primarily at or near the plasma membrane in all cell types examined. Two-color fluorescence analysis of Gag-TC in HeLa cells disclosed that nascent Gag was present mostly at the plasma membrane. The FlAsH-EDT_2-TC binding complex has been adapted for the stable, sensitive, and specific molecular tagging of HIV-1 for tracking incoming viral particles inside infected living cells.[50]

However, the use of ReAsH might cause temporary changes in cell morphology 24 to 48 h after labeling. These phenotypical transformations are presumably stimulated by the generation of singlet oxygen from ReAsH as a result of illumination by a high-intensity light source.[51] This has also been observed in fluorophore-assisted light inactivation experiments, again due to the production of reactive oxygen species (ROS).[52]

Recombinant connexin43 (Cx43) was expressed with a small TC peptide motif (Cx43-TC). Proteins of different ages could be sequentially labeled in living cells with differently colored biarsenical fluorophores; older and younger protein molecules could be clearly distinguished by fluorescence microscopy.[53] HeLa cells expressing Cx43-TC at their surface can be specifically labeled by FlAsH or ReAsH. Gap junctions (GJs) are defined as the contact regions between adjacent cells that contain several closely packed membrane channels. Cx43-TC was used to label GJs with ReAsH.[54] It not only becomes fluorescent after binding ReAsH, but also photo-oxidizes to give selectively stained channels. In chromophore-assisted light inactivation (CALI), Cx43 and α_{1c} L-type calcium channels were

tagged with one or two small TC motifs that specifically bind ReAsH.[51]

The utilization of TC-tagged vesicular stomatitis virus for studies on virus entry, uncoating, assembly, and its emergence from infected cells has been achieved.[54] The TC motif could be employed further with ReAsH labeling for both live-cell imaging and photoconversion of diaminobenzidine to allow direct correlation of live-cell images.

The merger of the FlAsH technique with 1,2-bis(o-aminophenoxy)ethane-N,N,N′,N′-tetraacetic acid chelator for Ca^{2+} has been developed to produce Calcium Green FlAsH (CaGF; Scheme 3). This fast detection technique can locate intracellular Ca^{2+} concentration.[55] The fluorogenicity of the FlAsH technique increased approximately ten times upon selective binding with Ca^{2+}. This Ca^{2+} sensor was found to be ineffective in case of Mg^{2+}.

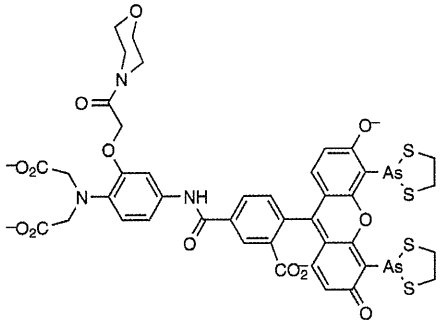

Scheme 3. Structure of CaGF.

The high affinity of a TC motif towards Zn^{2+} (with a significant binding strength) has been recently reported.[56] This high affinity results from the transfer of Zn^{2+} from its pool to TC motifs. This binding efficiency significantly decreased the binding interaction between TC and FlAsH-EDT_2 (and other biarsenicals).

3. Modification of SNAP-tag

Some articles in the last six years have described protein labeling with small molecules.[57–63] In these articles there are several examples of site-specific fluorescent labeling by probes within living cells. But the majority of these probes are nonfluorogenic in nature. One of such fluorescence labeling technique is the well-known SNAP-tag, a 20 kDa protein that has been used as a tag protein for specific labeling with O^6-benzylguanine (BG) derivatives.[19,62–67] To exploit the application of protein labeling technologies with combinations of synthetic probes, various photosensitive molecules have been used as probes in several applications. These photosensitive molecules need to be derivatized with BG substrates for SNAP-tag-induced protein-labeling methods. For effective FRET quenching, fluorophores and quenchers are chosen in such a way that the emission spectrum of the donor overlaps with the absorption spectrum of the quencher. This condition is a prerequisite for effective intramolecular quenching of a fluorophore by dynamic quenching mechanisms. This strategy has been applied for the generation of photoactivatable fluorophores that can be specifically sequestered to SNAP-tag fusion proteins. These probes are useful for the labeling of SNAP-tag fusion proteins, both on the cell surface and inside living cells.[68] Photoactivatable SNAP-tag fusion proteins have been applied to monitor protein mobility on the cell surface.

Fluorescence detection of physiologically active metal ions in selected organelles in live cells is of tremendous importance. For bioimaging studies, O^6-alkylguanine transferase (AGT) has been used to localize specific subcellular compartments.[19] In a recent approach, the AGT labeling methodology was combined with a known fluorescent zinc sensor to develop fusion proteins for the organelle-specific detection of Zn^{2+} in live cells. The target compound, ZP1BG, has a Zinpyr sensor and an AGT substrate, BG (Scheme 4). Live-cell imaging studies have demonstrated labeling by the probe in the Golgi apparatus and mitochondria.[69] Treatment with the probe in nontransfected cells confirmed the requirement for targeted AGT expression to obtain the staining pattern.

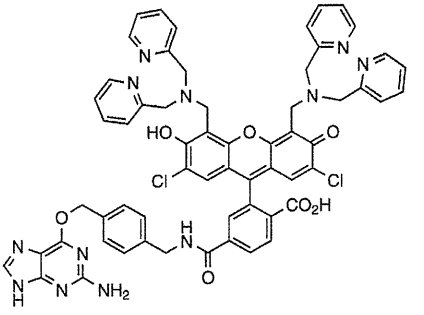

Scheme 4. Structure of ZP1BG.

The versatility of the SNAP-tag technology has been further exploited with small molecules on the surface or interior of living cells with the use of boronate-capped dyes for the specific visualization of H_2O_2. Appropriately derivatized boronates resulted in SNAP-Peroxy-Green (SNAP-PG, Scheme 5) probes after bioconjugation with SNAP-tag fusion proteins. The emission spectra of SNAP-PG suggested valid selective detection of H_2O_2 among other biologically relevant ROS.[70] Imaging experiments that used scanning confocal microscopy established the fluorogenicity of the SNAP-tag probes along with their organelle-specific localization with respect to the local H_2O_2 concentrations.

Recent progress in SNAP-tag methodology was the development of new class of cell permeable BODIPY-based Ca^{2+} indicators. The free indicator (BOCA-1) showed a significant fluorescence enhancement (250 times) after Ca^{2+} binding. The BG derivative, BOCA-1-BG (Scheme 6), was covalently and specifically linked to SNAP-tag fusion proteins in living cells. The fluorogenicity (180 times) of the indicator for Ca^{2+} binding was retained, even after conjugation to proteins.[71] BOCA-1-BG/SNAP-tag fusion proteins have proved useful in sensing

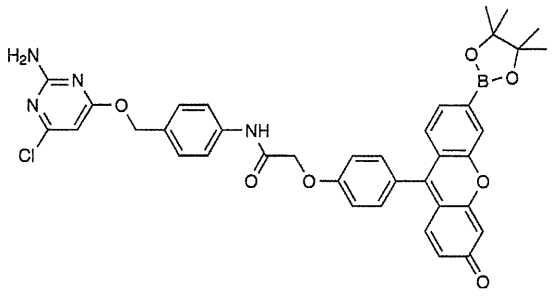

Scheme 5. Structure of SNAP-PG.

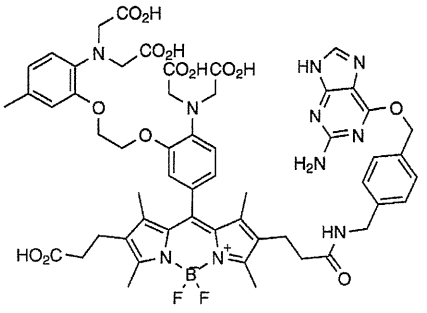

Scheme 6. Structure of BOCA-1-BG.

changes in Ca^{2+} concentrations in the nuclei and cytosol of live CHO-K1 cells. The high selectivity of the indicator-SNAP tag complex inside the living cells makes it a powerful tool for measuring local changes in Ca^{2+} concentrations.

4. BL-tag

β-Lactam antibiotics, such as penicillins and cephalosporins, have been routinely used in the treatment of bacterial infections over several decades. These antibacterial agents can inactivate (by the formation of stable covalent acyl complexes) penicillin-binding proteins that are responsible for synthesizing bacterial cell walls.[72–75] A sensitive and reagent-free biosensor for β-lactam antibiotics has been constructed from a modified class A β-lactamase.[76,77] This provided turn-on fluorescent biosensors for the direct detection of small ligands that can be constructed by placing fluorophores on flexible loops of enzyme mutants.

The reaction of TEM-1 (class A β-lactamases) with β- lactam rings involves acylation and deacylation steps. Glu166 is indispensable for the deacylation step; the mutant version of TEM-1 (BL) restricts the deacylation step (Scheme 7).[78,79] Our goal was to exploit the properties of BL for covalent attachment with a fluorescent substrate. In our protein-labeling method our aim was to combine fluorogenicity and specificity of the probe.

In our first attempt, we developed a novel protein-labeling system that involved the use of mutant β-lactamase and the specific probe CCD that exploits the principle of FRET (Scheme 8).[80] The two main features of our labeling system are control of the rate of substrate-leaving (to attain covalent binding of labeled compounds), and the fluorogenicity in the probe by successful triggering off the labeling step. Because of the rational design of both the tag protein and the labeling probe, this system enabled us to simultaneously achieve specific and fluorogenic labeling of the target protein.

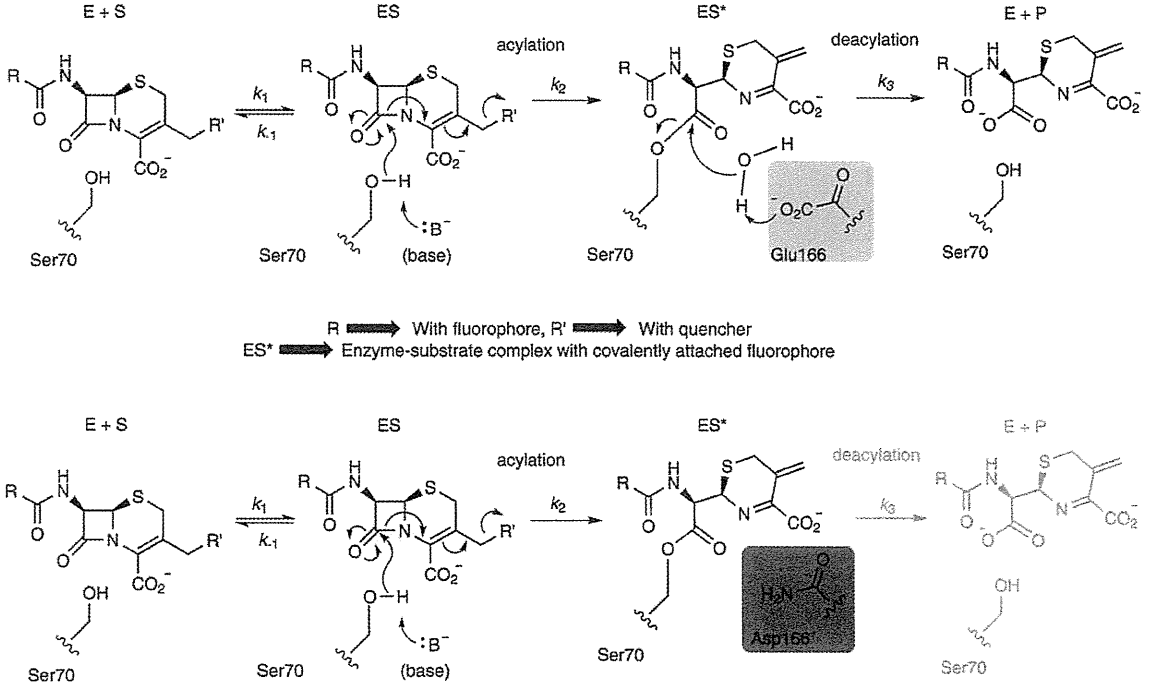

Scheme 7. General mechanism of the BL-tag technique by control of the deacylation step for protein labeling, with β-lactam cleavage by the mutant version (E166N) of class A β-lactamase. E: enzyme, S: substrate, P: product.

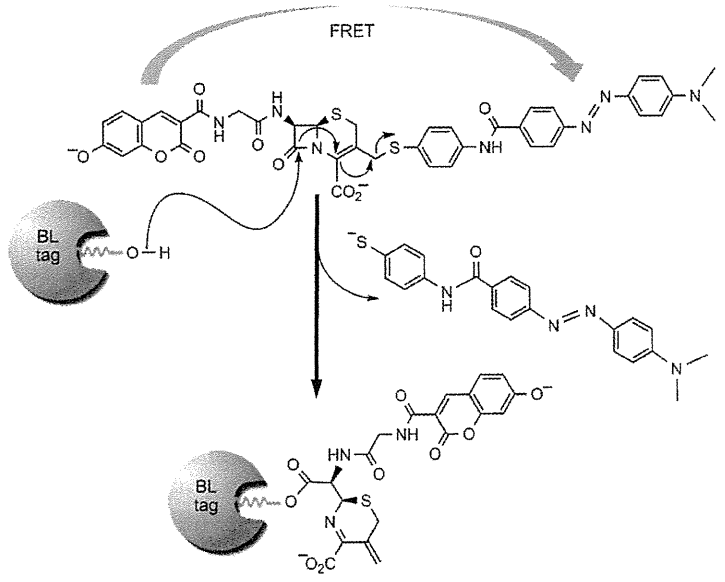

Scheme 8. Structure of CCD and its labeling strategy.

We reported a specific protein labeling system with a turn-on fluorescence switch. By using this system, we achieved specific and fluorogenic protein labeling under physiological conditions. In principle, this system does not require washing procedures to remove unreacted probes after labeling. We demonstrated the broad applicability of our BL-tag technology to live cell imaging by the development of a series of fluorescence labeling probes for this technology, and by examination of the functions of the target proteins. These new probes incorporated fluorescein (FCD, Figure 2) and rhodamine (RCDNB) chromophores. Each successfully yielded enhanced photophysical properties for cellular imaging. These probes were used to specifically label the BL-tag protein. BL-tag technology can be simultaneously used with other protein labeling methods such as SNAP-tag technology. Orthogonality of the substrate specificity between BL-tag and SNAP-tag was also demonstrated.[81] The function of epidermal growth factor receptor (EGFR) was found to be essentially preserved after the fusion of a BL-tag to its extracellular domain. This low interference with the functionality of the POI provides a great advantage over GFP fusion.

However, FRET-based fluorescence imaging has some drawbacks, including the unavailability of fluorescence quenchers for particular emission wavelengths. (The acceptor quencher's frequency needs to be specified according to the emission nature of the donor fluorophore). To surmount the limitations of the FRET process, our alternative approach, based on the switching mechanism, involved an "aggregation" process followed by an "elimination" process. We have recently developed a straightforward technique for protein-labeling systems (Scheme 9).[82,83] Here our target quencher was attached to the fluorophore by a long chain linker. The choice of quencher in this new technology is independent of the emission wavelength of the fluorophores, as supramolecular interactions are involved in quenching process. The efficiency of the quenching results from the aggregation process that has been found to be effective in physiological conditions. The design of the labeling probe (FCDNB) was based on elimination of the quencher part in the presence of an enzyme. The removal of quencher from the aggregation interaction resulted in recovery of the emission efficiency of the fluorophore. This fluorescence recovery has been employed in the protein labeling study.[82] Despite the similarity in molecular weight of BL and GFP, fluoro-

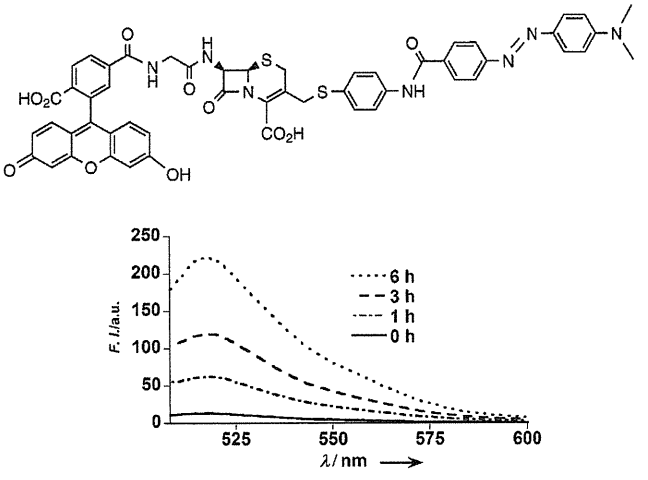

Figure 2. Structure of FCD and its fluorogenicity in presence of BL-tag.

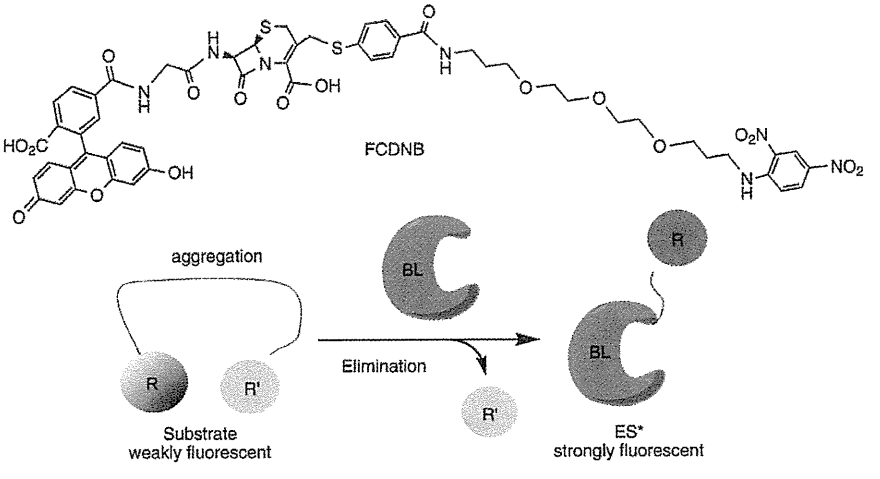

Scheme 9. Structure of FCDNB and its labeling strategy.

genicity can be introduced by BL-tag technology (virtually impossible with GFP). The viability of the fluorescently labeled BL-tag under physiological conditions has been explored with a newly designed and synthesized series of cephalosporin-based fluorescent probes. We found an order of labeling between the probes when a mixture of probe solutions was used. This ordering is a reflection of the control in the disaggregation step by the aggregation interaction between fluorophore and quencher.[83] We have extended the color range of fluorescence labeling probes with the high selectivity of the BL-tag technology, and demonstrate broad applicability of this labeling technology to live-cell imaging.

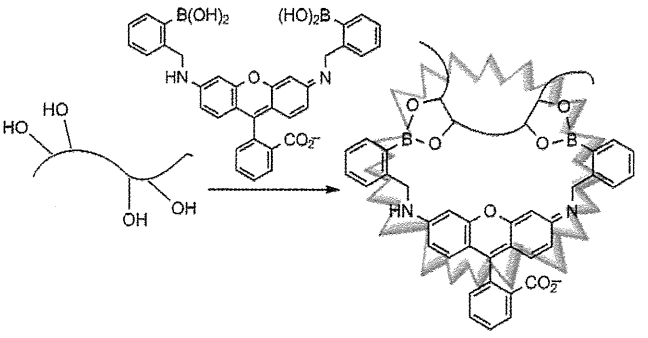

Scheme 11. Structure of the probe for the tetraserine-tag.

5. Other turn-on technique

Selective chemical labeling is generally achieved by site-specific binding between a tag (fused to a POI) and a small fluorescent compound, although some different approaches have also been reported. Several protein-mediated nonfluorogenic labeling methods, such as HaloTag,[84–87] tetraaspartate,[88,89] and α-bungarotoxin-binding peptide[90] are known in literature.

A fluorogenic probe that exhibits fluorescence spectral change upon labeling of the target enzyme, β-galacotosidase (β-gal), in living cells has been reported. The probe is a substrate of β-gal and is conjugated to fluorophores 7-hydroxycoumarin and fluorescein by a smartly designed linker that contains a quinone methide-forming molecule and a carbamate leaving group (Scheme 10).[91] The resultant labeled β-gal thus displays a fluorescence spectrum different from its initial emission maximum. This spectral change can report in real time the formation of labeled products in the presence of unlabeled protein and probe.

RhoBo, a rhodamine-derived bisboronic acid (Scheme 11) can function as a cell permeable, turn-on fluorescent sensor

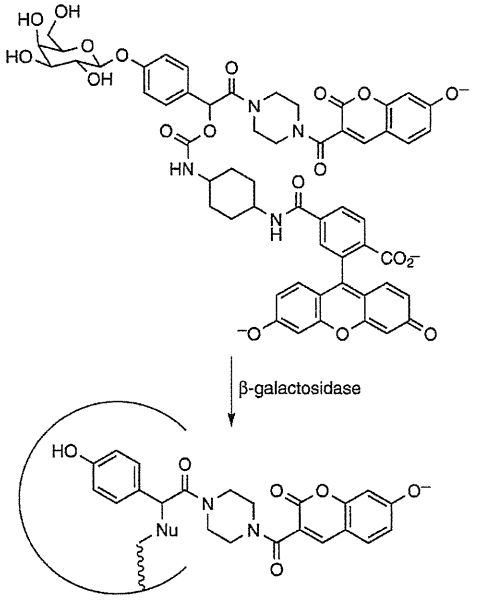

Scheme 10. Structure of the probe for the β-galacotosidase tag.

for tetraserine motifs in engineered proteins.[92] RhoBo dye showed higher affinity complexes with proteins that contain a linear tetraserine motif. The dye was chosen as it has the benefits of simple synthesis and low monosaccharide affinity, and it forms boronate esters that emit at longer wavelengths. The equilibrium stability and brightness of the RhoBo-peptide (Ac-WDSSPGSSK-NH_2) complex can be comparable to the complex formed between ReAsH-EDT_2 and FLNCCPGCCMEP. The affinity of RhoBo was also examined for other simple monosaccharides to evaluate the extent of competition between hydroxyl-rich functionalities and protein tetraserine motifs. The effects of monosaccharides were only observed when they were incubated in large excess (10000 times peptide concentration).

Haloalkane dehalogenase (HD) catalyzes the hydrolysis of haloalkanes by a covalent enzyme–substrate intermediate. Fusing a target protein to an HD variant that cannot hydrolyze the intermediate enabled labeling of the target protein with a haloalkane in vivo. The use of a fluorogenic tag that labels an HD variant in cellulo after unmasking by an intracellular esterase has been developed. Labeling was rapid and specific, as expected from enzymatic catalysts and from the high membrane permeance of the probe both before and after unmasking.[93]

Protein labeling based on a specific chelation has some remarkable features;[94,95] these include simplicity of the labeling procedures, highly selective and stable labeling (based on metal chelation), and applicability to various site-specific labeling tasks. An oligohistidine sequence (His_n, $n \geq 6$, in general) called His-tag is known to interact robustly with transition-metal complexes, including a nitrilotriacetic acid (NTA) complex of Ni^{2+}.[96–98] This sequence is widely used for the purification of expressed proteins by affinity chromatography. One of the major limitations in His-tag/NTA-Ni^{2+} system is the relatively low affinity between the His-tag and the NTA-Ni^{2+} complex; this property probably disturbs stable labeling and imaging. Analytical size exclusion chromatography shows that the binding stability increases substantially with an increasing number of NTA moieties.

In some site-specific labeling strategies, the labeled product loses its function upon covalent attachment to the ligand.[99–100] To overcome this problem, a new method has been developed for the site-selective attachment of synthetic molecules into specific "endogenous" proteins in vivo by using

ligand-directed tosyl (LDT) chemistry. Here the probe reacts with target proteins without yielding covalent protein-ligand adducts. In this process, an affinity ligand is connected to a probe by an electrophilic phenylsulfonate ester group; this results in the concomitant release of the ligand molecule when it interacts with the POI. At the same time the surface of the POI is specifically labeled by an S_N2-type reaction (Scheme 12). The proof of principle was tested with carbonic anhydrase (CA) as the POI, benzenesulfonamide as the specific ligand, and a coumarin-based dye as the probe. This approach has been applied not only for chemically labeling proteins in living cells, tissue, and mice, but also for constructing a biosensor directly inside cells without genetic engineering.[101] This LDT chemistry can be used as a new tool for the study and manipulation of biological systems.

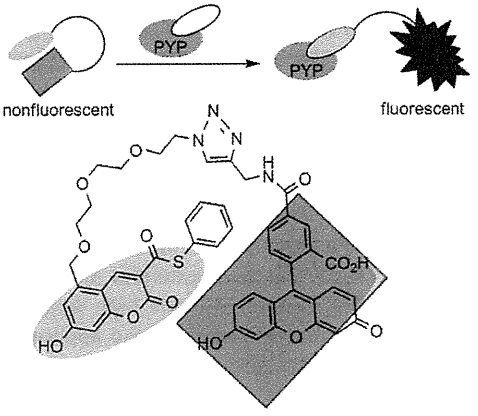

Scheme 13. Structure of the probe for the PYP-tag, and schematic strategy.

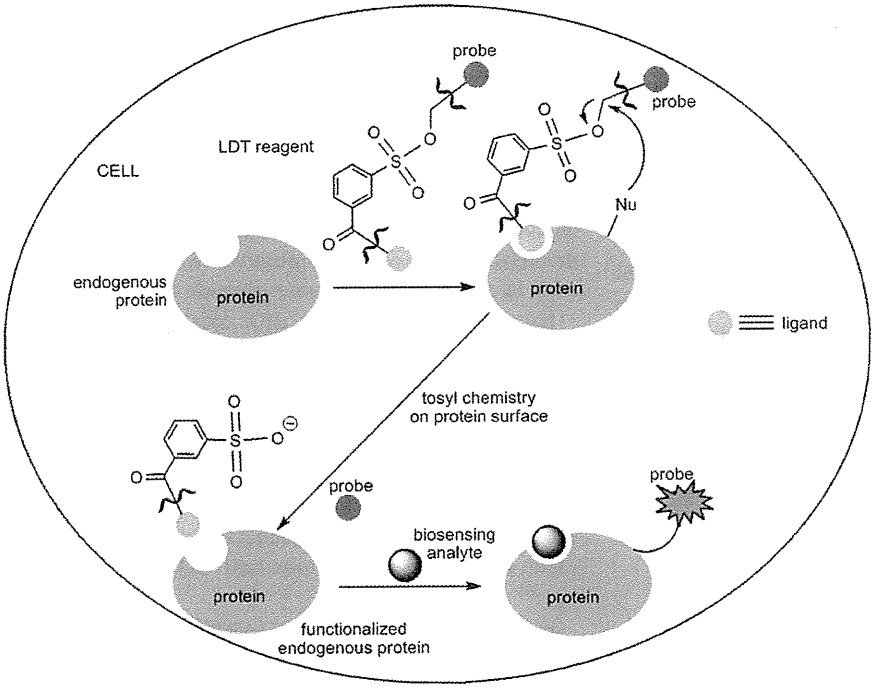

Scheme 12. LDT chemistry for labeling endogenous proteins in living native cells. Schematic illustration of the strategy.

Recently we have developed a protein labeling system that is based on a small tag protein, photoactive yellow protein (PYP), and its fluorescent probes.[102] Live-cell imaging and specific labeling of PYP were achieved by using a small fluorescein-based molecule (FCTP; Scheme 13). The designed FCTP probe contains two fluorophores that associate with each other by an intramolecular interaction, thereby leading to quenching of both fluorophores. One of the fluorophore works as a binding moiety with PYP, and the other behaves as a fluorescent signaling unit. The mechanism involved in the fluorogenic protein labeling triggers the dissociation of the quenched fluorophores, and enhanced fluorescence intensity of one fluorophore at the desired wavelength. This fluorogenic characteristic allows the identification of the probe bound to its protein tag. These properties offer a more sophisticated application of this system to protein imaging studies.

6. Outlook

Protein labeling with small photoactivatable probes is still a challenging job for chemical biologists who wish to interpret mechanistic details of protein functions. There are several examples of such labeling in vitro, but without any success in living systems. At this stage we can highlight some of the studies that might provide some concrete experimental evidence for protein function. One such work is based on PRIME (probe incorporation mediated by enzymes),[103] a method for fluorescent labeling of peptide-fused recombinant proteins in living cells with high specificity. This methodology involves an engineered fluorophore ligase that is derived from the natural *E. coli* enzyme lipoic acid ligase (LplA). Mutagenesis of this produces a mutant ligase capable of attaching a 7-hydroxycoumarin substrate, and it catalyzes the covalent linkage with a permutable LAP (LplA acceptor peptide) amino acid sequence. This fluorophore ligation process is very fast and has been found to be highly specific for LAP fusion proteins over all endogenous mammalian proteins.

In another approach, trypsin can be detected from homogeneous protein mixtures by a newly developed conjugated polymer-fluorescent probe based platform.[104] This method has the advantage of correct detection of the specific interaction

between the probe and the active site of trypsin. Possible energy transfer between the polymer and the probe is due to the electrostatic interaction between the polymer and protein.

A recent report describes the steric factors of the substituents that play an important part in binding of the squaraine dyes with serum albumins.[105] These dyes, with the help of the synergistic effects of hydrophobic, hydrogen bonding, and electrostatic interactions, show turn-on fluorescence upon site-selective binding of the transport proteins. This indicates the potential use of these dyes as NIR noncovalent protein labeling and photodynamic therapeutic agents. The potential application of "turn on" type protein labeling has a bright prospect in future research.

Acknowledgements

Part of the research in our lab is supported by the Japan Society for the Promotion of Science (JSPS) through its "Funding Program for World-Leading Innovative R&D on Science and Technology (FIRST Program). This work was supported in part by the CREST funding program from Japan Science and Technology Agency (JST), the Grant-in-Aid for Scientific Research from the Ministry of Education, Culture, Sports, Science and Technology (MEXT) of Japan, and the Grant-in-Aid from the Ministry of Health, Labour and Welfare (MHLW) of Japan. K.K.S. acknowledges support from a Global COE Fellowship of Osaka University.

Keywords: biotechnology · dyes · fluorescence spectroscopy · fluorescent probes · protein labeling

[1] K. M. Marks, G. P. Nolan, *Nat. Methods* **2006**, *3*, 591–596.
[2] M. J. Hinner, K. Johnsson, *Curr. Opin. Biotechnol.* **2010**, *21*, 766–776.
[3] O. Shimomura, F. H. Johnson, Y. Saiga, *J. Cell. Comp. Physiol.* **1962**, *59*, 223–239.
[4] J. G. Morin, J. W. Hastings, *J. Cell. Physiol.* **1971**, *77*, 305–312.
[5] J. G. Morin, J. W. Hastings, *J. Cell. Physiol.* **1971**, *77*, 313–318.
[6] R. Heim, D. C. Prasher, R. Y. Tsien, *Proc. Natl. Acad. Sci. USA* **1994**, *91*, 12501–12504.
[7] D. C. Prasher, V. K. Eckenrode, W. W. Ward, F. G. Prendergast, M. J. Cormier, *Gene* **1992**, *111*, 229–233.
[8] C. W. Cody, D. C. Prasher, W. M. Westler, F. G. Prendergast, W. W. Ward, *Biochemistry* **1993**, *32*, 1212–1218.
[9] O. Shimomura, *FEBS Lett.* **1979**, *104*, 220–222.
[10] R. Y. Tsien, *Annu. Rev. Biochem.* **1998**, *67*, 509–544.
[11] R. Y. Tsien, *FEBS Lett.* **2005**, *579*, 927–932.
[12] N. C. Shaner, P. A. Steinbach, R. Y. Tsien, *Nat. Methods* **2005**, *2*, 905–909.
[13] J. Lippincott-Schwartz, G. H. Patterson, *Science* **2003**, *300*, 87–91.
[14] J. Zhang, R. E. Campbell, A. Y. Ting, R. Y. Tsien, *Nat. Rev. Mol. Cell Biol.* **2002**, *3*, 906–918.
[15] A. Miyawaki, J. Llopis, R. Heim, J. M. McCaffery, J. A. Adams, M. Ikura, R. Y. Tsien, *Nature* **1997**, *388*, 882–887.
[16] D. Marguet, E. T. Spiliotis, T. Pentcheva, M. Lebowitz, J. Schneck, M. Edidin, *Immunity* **1999**, *11*, 231–240.
[17] C. S. Lisenbee, S. K. Karnik, R. N. Trelease, *Traffic* **2003**, *4*, 491–501.
[18] N. C. Shaner, R. E. Campbell, P. A. Steinbach, B. N. Giepmans, A. E. Palmer, R. Y. Tsien, *Nat. Biotechnol.* **2004**, *22*, 1567–1572.
[19] A. Keppler, S. Gendreizig, T. Gronemeyer, H. Pick, H. Vogel, K. Johnsson, *Nat. Biotechnol.* **2003**, *21*, 86–89.
[20] L. W. Miller, Y. Cai, M. P. Sheetz, V. W. Cornish, *Nat. Methods* **2005**, *2*, 255–257.
[21] M. Fernández-Suárez, A. Y. Ting, *Nat. Rev. Mol. Cell Biol.* **2008**, *9*, 929–943.
[22] J. Farinas, A. S. Verkman, *J. Biol. Chem.* **1999**, *274*, 7603–7606.
[23] S. P. Sasso, R. M. Gilli, J. C. Sari, O. S. Rimet, C. M. Briand, *Biochim. Biophys. Acta Protein Struct. Mol. Enzymol.* **1994**, *1207*, 74–79.
[24] T. Clackson, W. Yang, L. W. Rozamus, M. Hatada, J. F. Amara, C. T. Rollins, L. F. Stevenson, S. R. Magari, S. A. Wood, N. L. Courage, X. Lu, F. Cerasoli, Jr., M. Gilman, D. A. Holt, *Proc. Natl. Acad. Sci. USA* **1998**, *95*, 10437–10442.
[25] L. W. Miller, J. Sable, P. Goelet, M. P. Sheetz, V. W. Cornish, *Angew. Chem.* **2004**, *116*, 1704–1707; *Angew. Chem. Int. Ed.* **2004**, *43*, 1672–1675.
[26] K. M. Marks, P. D. Braun, G. P. Nolan, *Proc. Natl. Acad. Sci. USA* **2004**, *101*, 9982–9987.
[27] M. Robers, P. Pinson, L. Leong, R. H. Batchelor, K. R. Gee, T. Machleidt, *Cytometry A* **2009**, *75A*, 207–224.
[28] T. Machleidt, M. Robers, G. T. Hanson, *Methods Mol. Biol.* **2007**, *356*, 209–220; D. L. Taylor, J. R. Haskins, K. Giuliano, *High Content Screening: A Powerful Approach to Systems Cell Biology and Drug Discovery*, Humana Press, Totowa, **2007**.
[29] B. A. Griffin, S. R. Adams, R. Y. Tsien, *Science* **1998**, *281*, 269–272.
[30] B. A. Griffin, S. R. Adams, J. Jones, R. Y. Tsien, *Methods Enzymol.* **2000**, *327*, 565–578.
[31] S. R. Adams, R. E. Campbell, L. A. Gross, B. R. Martin, G. K. Walkup, Y. Yao, J. Llopis, R. Y. Tsien, *J. Am. Chem. Soc.* **2002**, *124*, 6063–6076.
[32] H. Yang, J. He, F. Hu, C. Zheng, Z. Yu, *Bioconjugate Chem.* **2010**, *21*, 1341–1348.
[33] K. S. Thorn, N. Naber, M. Matuska, R. D. Vale, R. Cooke, *Protein Sci.* **2000**, *9*, 213–217.
[34] B. R. Martin, B. N. G. Giepmans, S. R. Adams, R. Y. Tsien, *Nat. Biotechnol.* **2005**, *23*, 1308–1314.
[35] K. W. Marek, G. W. Davis, *Neuron* **2002**, *36*, 805–813.
[36] R. G. Panchal, G. Ruthel, T. A. Kenny, G. H. Kallstrom, D. Lane, S. S. Badie, L. Li, S. Bavari, M. J. Aman, *Proc. Natl. Acad. Sci. USA* **2003**, *100*, 15936–15941.
[37] C. Hoffmann, G. Gaietta, M. Bünemann, S. R. Adams, S. Oberdorff-Maass, B. Behr, J.-P. Vilardaga, R. Y. Tsien, M. H. Ellisman, M. J. Lohse, *Nat. Methods* **2005**, *2*, 171–176.
[38] B. M. Coleman, R. M. Nisbet, S. Han, R. Cappai, D. M. Hatters, A. F. Hill, *Biochem. Biophys. Res. Commun.* **2009**, *380*, 564–568.
[39] Y. Taguchi, Z.-D. Shi, B. Ruddy, D. W. Dorward, L. Greene, G. S. Baron, *Mol. Biol. Cell* **2009**, *20*, 233–244.
[40] S. B. Van Engelenburg, A. E. Palmer, *Chem. Biol.* **2008**, *15*, 619–628.
[41] J. Nakanishi, T. Nakajima, M. Sato, T. Ozawa, K. Tohda, Y. Umezawa, *Anal. Chem.* **2001**, *73*, 2920–2928.
[42] J. C. Goldstein, C. Muñoz-Pinedo, J.-E. Ricci, S. R. Adams, A. Kelekar, M. Schuler, R. Y. Tsien, D. R. Green, *Cell Death Differ.* **2005**, *12*, 453–462.
[43] B. Chen, H. Cao, P. Yan, M. U. Mayer, T. C. Squier, *Bioconjugate Chem.* **2007**, *18*, 1259–1265.
[44] A. Zürn, C. Klenk, U. Zabel, S. Reiner, M. J. Lohse, C. Hoffmann, *Bioconjugate Chem.* **2010**, *21*, 853–859.
[45] S. R. Adams, R. Y. Tsien, *Nat. Protoc.* **2008**, *3*, 1527–1534.
[46] C. Hoffmann, G. Gaietta, A. Zürn, S. R. Adams, S. Terrillon, M. H. Ellisman, R. Y. Tsien, M. J. Lohse, *Nat. Protoc.* **2010**, *5*, 1666–1677.
[47] R.-D. Hwang, C.-C. Chen, D. A. Knecht, *J. Microsc.* **2009**, *234*, 9–15.
[48] C. A. Wurm, I. E. Suppanz, S. Stoldt, S. Jakobs, *J. Microsc.* **2010**, *240*, 6–13.
[49] L. Rudner, S. Nydegger, L. V. Coren, K. Nagashima, M. Thali, D. E. Ott, *J. Virol.* **2005**, *79*, 4055–4065.
[50] N. J. Arhel, P. Charneau, *Methods in Molecular Biology Vol. 485: HIV Protocols*, 2nd ed. (Eds.: V. R. Prasad, G. V. Kalpana), Humana, Totowa, **2009**, pp. 151–159.
[51] O. Tour, R. M. Meijer, D. A. Zacharias, S. R. Adams, R. Y. Tsien, *Nat. Biotechnol.* **2003**, *21*, 1505–1508.
[52] G. Gaietta, T. J. Deerinck, S. R. Adams, J. Bouwer, O. Tour, D. W. Laird, G. E. Sosinsky, R. Y. Tsien, M. H. Ellisman, *Science* **2002**, *296*, 503–507.
[53] G. E. Sosinsky, G. M. Gaietta, G. Hand, T. J. Deerinck, A. Han, M. Mackey, S. R. Adams, J. Bouwer, R. Y. Tsien, M. H. Ellisman, *Cell Commun. Adhes.* **2003**, *10*, 181–186.
[54] S. C. Das, D. Panda, D. Nayak, A. K. Pattnaik, *J. Virol.* **2009**, *83*, 2611–2622.

[55] O. Tour, S. R. Adams, R. A. Kerr, R. M. Meijer, T. J. Sejnowski, R. W. Tsien, R. Y. Tsien, *Nat. Chem. Biol.* **2007**, *3*, 423–431.
[56] A. Pomorski, J. Otlewski, A. Krężel, *ChemBioChem* **2010**, *11*, 1214–1218.
[57] I. Chen, A. Y. Ting, *Curr. Opin. Biotechnol.* **2005**, *16*, 35–40.
[58] L. W. Miller, V. W. Cornish, *Curr. Opin. Chem. Biol.* **2005**, *9*, 56–61.
[59] H. M. O'Hare, K. Johnsson, A. Gautier, *Curr. Opin. Struct. Biol.* **2007**, *17*, 488–494.
[60] A. Dragulescu-Andrasi, J. Rao, *ChemBioChem* **2007**, *8*, 1099–1101.
[61] E. M. Sletten, C. R. Bertozzi, *Angew. Chem.* **2009**, *121*, 7108–7133; *Angew. Chem. Int. Ed.* **2009**, *48*, 6974–6998.
[62] K. Johnsson, *Nat. Chem. Biol.* **2009**, *5*, 63–65.
[63] N. Johnsson, K. Johnsson, *ACS Chem. Biol.* **2007**, *2*, 31–38.
[64] M. Kindermann, I. Sielaff, K. Johnsson, *Bioorg. Med. Chem. Lett.* **2004**, *14*, 2725–2728.
[65] A. Keppler, H. Pick, C. Arrivoli, H. Vogel, K. Johnsson, *Proc. Natl. Acad. Sci. USA* **2004**, *101*, 9955–9959.
[66] A. Gautier, A. Juilleratk, C. Heinis, I. R. Corrêa Jr. , M. Kindermann, F. Beaufils, K. Johnsson, *Chem. Biol.* **2008**, *15*, 128–136.
[67] M. Bannwarth, I. R. Corrêa Jr. , M. Sztretye, S. Pouvreau, C. Fellay, A. Aebischer, L. Royer, E. Ríos, K. Johnsson, *ACS Chem. Biol.* **2009**, *4*, 179–190.
[68] D. Maurel, S. Banala, T. Laroche, K. Johnsson, *ACS Chem. Biol.* **2010**, *5*, 507–516.
[69] E. Tomat, E. M. Nolan, J. Jaworski, S. J. Lippard, *J. Am. Chem. Soc.* **2008**, *130*, 15776–15777.
[70] D. Srikun, A. E. Albers, C. I. Nam, A. T. Iavarone, C. J. Chang, *J. Am. Chem. Soc.* **2010**, *132*, 4455–4465.
[71] M. Kamiya, K. Johnsson, *Anal. Chem.* **2010**, *82*, 6472–6479.
[72] A. Matagne, A. Dubus, M. Galleni, J.-M. Frère, *Nat. Prod. Rep.* **1999**, *16*, 1–19.
[73] A. Matagne, J. Lamotte-Brasseur, J-M. Frère, *Biochem. J.* **1998**, *330*, 581–598.
[74] J. F. Fisher, S. O. Meroueh, S. Mobashery, *Chem. Rev.* **2005**, *105*, 395–424.
[75] M. S. Wilke, A. L. Lovering, N. C. J. Strynadka, *Curr. Opin. Microbiol.* **2005**, *8*, 525–533.
[76] P.-H. Chan, H.-B. Liu, Y. W. Chen, K.-C. Chan, C.-W. Tsang, Y.-C. Leung, K.-Y. Wong, *J. Am. Chem. Soc.* **2004**, *126*, 4074–4075.
[77] P.-H. Chan, P.-K. So, D.-L. Ma, Y. Zhao, T.-S. Lai, W.-H. Chung, K.-C. Chan, K.-F. Yiu, H.-W. Chan, F.-M. Siu, C.-W. Tsang, Y.-C. Leung, K.-Y. Wong, *J. Am. Chem. Soc.* **2008**, *130*, 6351–6361.
[78] G. Guillaume, M. Vanhove, J. Lamotte-Brasseur, P. Ledent, M. Jamin, B. Joris, J.-M. Frère, *J. Biol. Chem.* **1997**, *272*, 5438–5444.
[79] H. Adachi, T. Ohta, H. Matsuzawa, *J. Biol. Chem.* **1991**, *266*, 3186–3191.
[80] S. Mizukami, S. Watanabe, Y. Hori, K. Kikuchi, *J. Am. Chem. Soc.* **2009**, *131*, 5016–5017.
[81] S. Watanabe, S. Mizukami, Y. Hori, K. Kikuchi, *Bioconjugate Chem.* **2010**, *21*, 2320–2326.
[82] K. K. Sadhu, S. Mizukami, S. Watanabe, K. Kikuchi, *Chem. Commun.* **2010**, *46*, 7403–7405.
[83] K. K. Sadhu, S. Mizukami, S. Watanabe, K. Kikuchi, *Mol. BioSyst.* **2011**, *7*, 1766–1772.
[84] G. V. Los, A. Darzins, N. Karassina, C. Zimprich, R. Learish, M. G. McDougall, L. P. Encell, R. Friedman-Ohana, M. Wood, G. Vidugiris, K. Zimmerman, P. Otto, D. H. Klaubert, K. V. Wood, *Promega Cell Notes* **2005**, *11*, 2–6.
[85] G. V. Los, L. P. Encell, M. G. McDougall, D. D. Hartzell, N. Karassina, C. Zimprich, M. G. Wood, R, Learish, R. Friedman Ohana, M. Urh, D. Simpson, J. Mendez, K. Zimmerman, P. Otto, G. Vidugiris, J. Zhu, A. Darzins, D. H. Klaubert, R. F. Bulleit, K. V. Wood, *ACS Chem. Biol.* **2008**, *3*, 373–382.
[86] J. Schröder, H. Benink, M. Dyba, G. V. Los, *Biophys. J.* **2009**, *96*, L01–L03.
[87] R. Friedman Ohana, L. P. Encell, K. Zhao, D. Simpson, M. R. Slater, M. Urh, K. V. Wood, *Protein Expression Purif.* **2009**, *68*, 110–120.
[88] A. Ojida, K. Honda, D. Shinmi, S. Kiyonaka, Y. Mori, I. Hamachi, *J. Am. Chem. Soc.* **2006**, *128*, 10452–10459.
[89] H. Nonaka, S. Tsukiji, A. Ojida, I. Hamachi, *J. Am. Chem. Soc.* **2007**, *129*, 15777–15779.
[90] Y. Sekine-Aizawa, R. L. Huganir, *Proc. Natl. Acad. Sci. USA* **2004**, *101*, 17114–17119.
[91] T. Komatsu, K. Kikuchi, H. Takakusa, K. Hanaoka, T. Ueno, M. Kamiya, Y. Urano, T. Nagano, *J. Am. Chem. Soc.* **2006**, *128*, 15946–15947.
[92] T. L. Halo, J. Appelbaum, E. M. Hobert, D. M. Balkin, A. Schepartz, *J. Am. Chem. Soc.* **2009**, *131*, 438–439.
[93] R. W. Watkins, L. D. Lavis, V. M. Kung, G. V. Los, R. T. Raines, *Org. Biomol. Chem.* **2009**, *7*, 3969–3975.
[94] D. W. Domaille, E. L. Que, C. J. Chang, *Nat. Chem. Biol.* **2008**, *4*, 168–175.
[95] N. Soh, *Sensors* **2008**, *8*, 1004–1024.
[96] N. Soh, D. Seto, K. Nakano, T. Imato, *Mol. BioSyst.* **2006**, *2*, 128–131.
[97] M. Kamoto, N. Umezawa, N. Kato, T. Higuchi, *Chem. Eur. J.* **2008**, *14*, 8004–8012.
[98] M. Kamoto, N. Umezawa, N. Kato, T. Higuchi, *Bioorg. Med. Chem. Lett.* **2009**, *19*, 2285–2288.
[99] M. S. Cohen, C. Zhang, K. M. Shokat, J. Taunton, *Science* **2005**, *308*, 1318–1321.
[100] Y. Takaoka, H. Tsutsumi, N. Kasagi, E. Nakata, I. Hamachi, *J. Am. Chem. Soc.* **2006**, *128*, 3273–3280.
[101] S. Tsukiji, M. Miyagawa, Y. Takaoka, T. Tamura, I. Hamachi, *Nat. Chem. Biol.* **2009**, *5*, 341–343.
[102] Y. Hori, H. Ueno, S. Mizukami, K. Kikuchi, *J. Am. Chem. Soc.* **2009**, *131*, 16610–16611.
[103] C. Uttamapinant, K. A. White, H. Baruah, S. Thompson, M. Fernández-Suárez, S. Puthenveetil, A. Y. Ting, *Proc. Natl. Acad. Sci. USA* **2010**, *107*, 10914–10919.
[104] Q. Zhu, R. Zhan, B. Liu, *Macromol. Rapid Commun.* **2010**, *31*, 1060–1064.
[105] V. S. Jisha, K. T. Arun, M. Hariharan, D. Ramaiah, *J. Phys. Chem. B* **2010**, *114*, 5912–5919.

Received: February 28, 2011
Published online on May 31, 2011

Bioorganic & Medicinal Chemistry 20 (2012) 769–774

Contents lists available at SciVerse ScienceDirect

Bioorganic & Medicinal Chemistry

journal homepage: www.elsevier.com/locate/bmc

Switchable MRI contrast agents based on morphological changes of pH-responsive polymers

Satoshi Okada [a], Shin Mizukami [a,b], Kazuya Kikuchi [a,b,*]

[a] Division of Advanced Science and Biotechnology, Graduate School of Engineering, Osaka University, 2-1 Yamadaoka, Suita, Osaka 565-0871, Japan
[b] Immunology Frontier Research Center, Osaka University, 3-1 Yamadaoka, Suita, Osaka 565-0871, Japan

ARTICLE INFO

Article history:
Received 26 October 2011
Revised 30 November 2011
Accepted 1 December 2011
Available online 8 December 2011

Keywords:
MRI
Contrast agent
pH-responsive polymer
Rotational correlation time
Molecular switch

ABSTRACT

Magnetic resonance imaging (MRI) contrast agents are effective tools in both medical diagnosis and life science research. Various smart contrast agents have been developed for the visualization of biological phenomena. These contrast agents have molecular switches that increase or reduce MRI signal intensity in response to the target biological reaction. Therefore, novel approaches to the design of molecular switches for versatile in vivo studies using MRI are eagerly anticipated. Here, we report one such approach for the development of molecular switches based on morphological changes of pH-responsive polymers. We designed and synthesized three types of contrast agents based on a linear homopolymer or spherical copolymers with two different cross-linking degrees. The relaxivity measurements showed that these agents have molecular switches that respond to pH changes, and fluorescence studies indicated that these switches are based on the alteration of the molecular tumbling caused by pH-responsive morphological changes. As a result, the spherical polymers possess promising characteristics for the development of switchable MRI contrast agents.

1. Introduction

Magnetic resonance imaging (MRI) is a useful imaging method because it allows for the noninvasive visualization of living tissues with high spatial and temporal resolution. MRI contrast agents (CAs) are widely used in medical diagnosis to improve the tissue contrast by shortening the longitudinal relaxation time (T_1) and the transverse relaxation time (T_2) of water protons. T_1 and T_2 shortening efficiencies of the CA are described as T_1 relaxivity (r_1) and T_2 relaxivity (r_2), respectively.[1,2] Thus, higher relaxivity means higher sensitivity of the CA, which results in significant changes in the MRI signal intensity.

Recently, switchable CAs have been used to detect enzyme reactions,[3,4] metal ions,[5,6] and pH alteration.[7–10] These so-called 'smart' CAs contain molecular switches, which cause their relaxivities to change in response to the targeted biological reaction. One common approach to the development of molecular switches is to change the coordination number of water molecules. In this case, the coordination of a water molecule with the paramagnetic ion is obstructed by the removable or coordinating group.[3,5,6] After stimulation, these hindrances to the coordination of the water molecule are eliminated, and the relaxivity increases. Another approach is based on the molecular tumbling of the CA. It is known that the rotational correlation time (τ_R), which is an indicator of the velocity of molecular tumbling in the solution, affects the relaxivity. In general, slower molecular tumbling (larger τ_R) results in increased relaxivity. In this way, the stimuli-responsive self-assembly of CAs, or the binding of CAs to macromolecules, act as molecular switching processes.[4,8–10]

Intelligent polymers have been developed for various biomedical applications, including drug delivery carriers,[11,12] imaging tools,[13,14] bio-mimic antibodies,[15] and antibacterial agents.[16] Their intelligent behaviors are also applicable to the development of switchable CAs and can be divided broadly into two types of behaviors, resulting from either linear or spherical polymers.

Previously, we applied the morphological change of a linear polymer to the development of a pH-responsive CA.[10] Although spherical polymers also have significant potential to develop switchable CAs, their applicability in this arena has not yet been examined. Herein, we demonstrate that pH-responsive morphological changes of spherical polymers can act as a molecular switching process. Three types of CAs were synthesized using one linear and two different spherical polymers. The relaxivities of these CAs were in fact dependent upon pH. The fluorescence studies indicated that the molecular switch is based on the alteration of the molecular tumbling caused by the pH-responsive morphological changes.

* Corresponding author. Tel.: +81 6 6879 7924; fax: +81 6 6879 7875.
E-mail address: kkikuchi@mls.eng.osaka-u.ac.jp (K. Kikuchi).

0968-0896/$ - see front matter © 2011 Elsevier Ltd. All rights reserved.
doi:10.1016/j.bmc.2011.12.005

2. Results and discussion

2.1. Development of pH-responsive CAs

2.1.1. Design, synthesis, and characterization

To establish a new approach for the development of switchable CAs, we designed three types of pH-responsive CAs, namely **H-Gd**, **C10-Gd**, and **C30-Gd** (Fig. 1). These CAs are based on anionic pH-responsive polymers with Gd^{3+} complexes and dansyl fluorophores. Because it is based on a non-cross-linked homopolymer, the structure of **H-Gd** is considered to be linear. In contrast, **C10-Gd** and **C30-Gd** are spherical structures based on 10% and 30% cross-linked copolymers, respectively. We expected that pH-responsive morphological changes of the polymers could act as molecular switches for the detection of pH change.

According to Scheme 1, we synthesized three types of pH-responsive CAs. Methacrylic acid (MAA) and *N*,*N*′-methylenebisacrylamide (MBAAm) were used as the monomer and cross-linker, respectively. First, non-cross-linked homopolymer PMAA and cross-linked copolymers C10 and C30 were synthesized by distillation precipitation polymerization.[17] The cross-linking degree was controlled by altering the weight of added MBAAm as the appropriate fraction of the combined weight of the monomer and cross-linker. **H-Gd**, **C10-Gd**, and **C30-Gd** were then synthesized by covalently-attaching both the aminoethyl-modified Gd(DO3A) complex [Gd(AEDO3A)],[18] which is a derivative of clinically-used $Gd(DOTA)^{-1}$ complexes, and dansyl ethylenediamine[19] to PMAA, C10, and C30, respectively (Table 1).

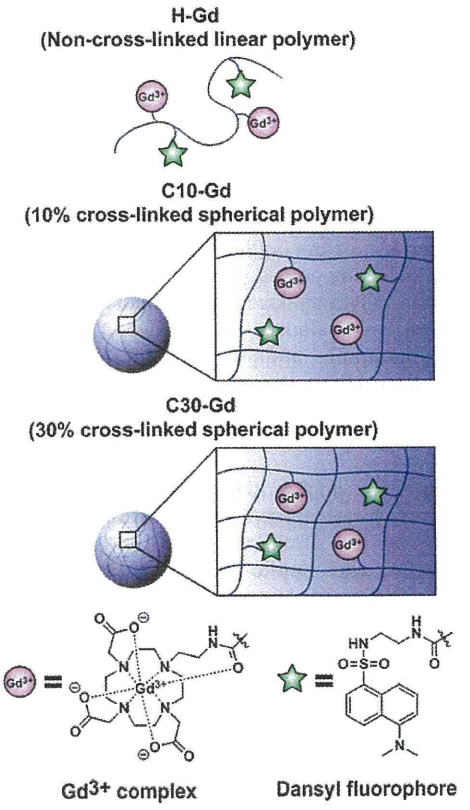

Figure 1. Design of pH-responsive CAs based on the linear homopolymer and cross-linked spherical polymers.

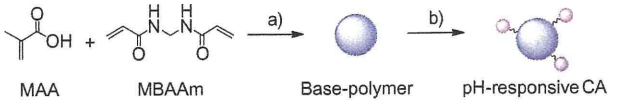

Scheme 1. Synthesis of pH-responsive CAs: (a) AIBN, CH_3CN. (b) Gd(AEDO3A), dansyl ethylenediamine, WSCD·HCl, HOBt, DIEA, DMF.

Table 1
Cross-linking degree, number-average diameter (D_n), weight-average diameter (D_W), polydispersity index (PDI), and Gd content of polymers

Entry	Cross-linking degree[a] (wt %)	D_n[b] (nm)	D_W[b] (nm)	PDI[b]	Gd content (wt %)
PMAA	0	108	114	1.055	0
H-Gd	0	—	—	—	0.21
C10-Gd	10	171	175	1.019	0.42
C30-Gd	30	105	106	1.012	0.45

[a] Calculated from elemental analysis data.
[b] Calculated from TEM images based on the following equation:[17]

$$D_n = \sum_{i=1}^{k} n_i D_i / \sum_{i=1}^{k} n_i ; D_w \sum_{i=1}^{k} n_i D_i^4 / \sum_{i=1}^{k} n_i D_i^3 ; \mathrm{PDI} = D_w / D_n$$

These values reflect the 100 particles from TEM micrographs.

The dispersities, geometries, and average diameters of the synthesized CAs were characterized by transmission electron microscopy (TEM) (Fig. 2 and Table 1). The TEM images showed monodisperse spherical shapes of **C10-Gd** and **C30-Gd**. **H-Gd** was not observed by TEM since it was not cross-linked and was thus expected to become uncoiled during the synthesis and purification process; however, the TEM image of its precursor PMAA was observed. The pH-responses of **C10-Gd** and **C30-Gd** were analyzed under various pH conditions with dynamic light scattering (DLS) (Fig. 3), which showed that the hydrodynamic diameters of **C10-Gd** and **C30-Gd** decreased with decreasing pH. The pH-response of **C10-Gd** was larger than that of **C30-Gd** due to the lower degree of cross-linking of **C10-Gd**. The amount of Gd in each of the polymers was quantified by inductively coupled plasma mass spectrometry (ICP-MS).

2.1.2. Relaxivity measurements

In order to study the function of **H-Gd**, **C10-Gd**, and **C30-Gd** as switchable CAs, we measured their relaxivities using a 0.47 T nuclear magnetic resonance (NMR) analyzer under various pH conditions (Fig. 4). Both r_1 and r_2 of all three polymers increased with decreasing pH, meaning that they all act as pH-responsive CAs and could detect a low pH. The spherical **C10-Gd** and **C30-Gd** showed more drastically varying relaxivity pH-responses than did **H-Gd**. It was also observed that the relaxivity was enhanced by an increase in the degree of cross-linking.

Previously, we developed a pH-responsive CA based on another linear polymer with carboxylate anionic groups.[10] In the study, it was indicated that the pH-responsive morphological conversion between the globular form and the extended form altered the molecular motion of the polymer side chains, and functioned as the molecular switch. The relaxivities of **H-Gd** showed quite similar pH-responsive behaviors to those of the previous polymer. Therefore, pH-responsive relaxometric behaviors of **H-Gd** were probably caused by the molecular motion switch.

The relaxivities of cross-linked spherical **C10-Gd** and **C30-Gd** also increased at low pH. The relaxivity values of the spherical polymers were much higher than those of the linear polymer and enhanced with increasing the cross-linking degree. These results indicate that spherical polymers have significant potential to be switchable CAs with high sensitivities. From DLS measurements, spherical polymers expressed pH-responsive shrinking-swelling behaviors (Fig. 3).

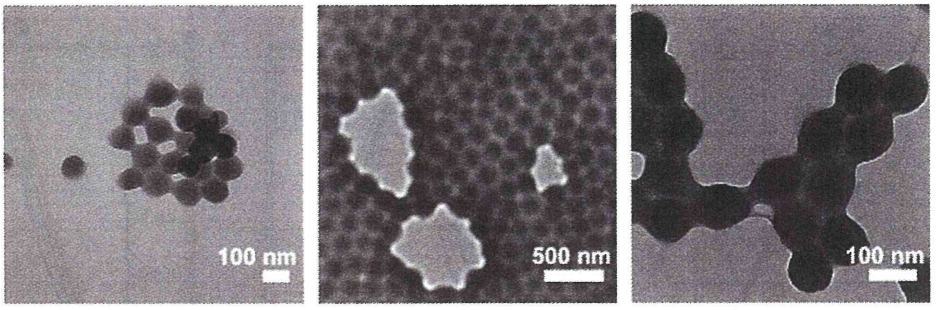

Figure 2. TEM images of PMAA (left), **C10-Gd** (middle), and **C30-Gd** (right).

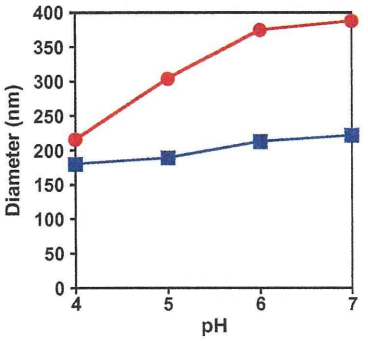

Figure 3. Hydrodynamic diameters of **C10-Gd** (circle symbol) and **C30-Gd** (square symbol) under various pH conditions at 25 °C.

It was assumed that these morphological changes affected the relaxivity. Therefore, the correlations among relaxivities, morphological behaviors, and rotational motions were thoroughly investigated in the following sections (Sections 2.2 and 2.3).

2.2. Elucidation of pH-responsive morphological changes by fluorescence studies

2.2.1. Fluorescence spectra measurements

The dansyl group is an environmentally-sensitive fluorophore that is suitable for observing the pH-response of polymers, because its emission wavelength is blue-shifted as the surrounding hydrophobicity increases, but is negligibly affected by the solution pH.[10,20,21] In order to monitor the pH-responsive morphological change, we measured the fluorescence spectra (Fig. 5). In all polymers, the emission spectra were blue-shifted at a low pH, indicating that the dansyl groups were surrounded by more hydrophobic environment at a low pH. It was expected that **H-Gd** would be a globular structure at a low pH. From the DLS measurements, spherical **C10-Gd** and **C30-Gd** were shown to gradually shrink with a decreasing pH. Thus, it was expected that the increased hydrophobicity of the internal space at a low pH was a result of decreasing the polymer mesh size. The pH-response of **C30-Gd** was smaller compared with the others because its structure is more rigid, owing to its high degree of cross-linking. Interestingly, the wavelength shift of **C10-Gd** was more similar to that of **H-Gd**, rather than **C30-Gd**.

2.2.2. Fluorescence lifetime measurements

The fluorescence lifetime of dansyl fluorophores in the hydrophobic and hydrophilic environments respectively expresses long and short lifetimes.[22] Therefore, the fluorescence lifetime analysis provides the morphological information about the polymer with dansyl groups. We measured the fluorescence decay curves of each of the three CAs at various pH conditions (Supplementary Fig. S1). The fluorescence decay curve of **H-Gd** consisted of two components (Table 2). The first is short lifetime, (~6.7 ns) and its fraction decreased with decreasing pH. The other component is long lifetime (~21.7 ns), which increased with decreasing pH. These results confirm that a higher number of dansyl groups are exposed to the hydrophobic environment as the pH decreases, since **H-Gd** is globular at a lower pH.

In the case of **C10-Gd** and **C30-Gd**, we eliminated the light-scattering lifetime from the calculations for the fractions of each fluorescence lifetime (Table 2). We found that the fluorescence decay parameters of **C10-Gd** were similar to those of **H-Gd**. Although **C10-Gd** is a cross-linked spherical polymer, the surrounding environment of dansyl groups is similar to that of dansyl groups

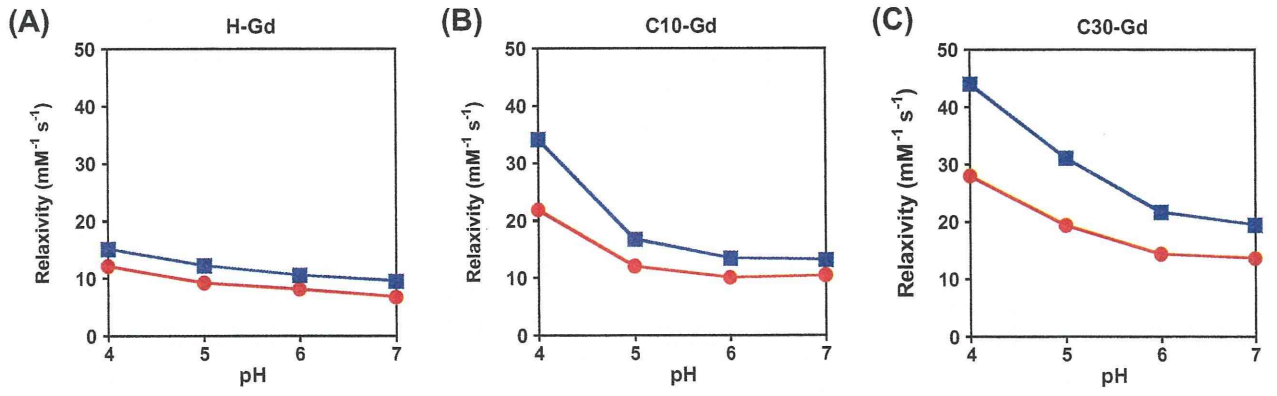

Figure 4. Longitudinal relaxivities (r_1) and transverse relaxivities (r_2) of **H-Gd** (A), **C10-Gd** (B), and **C30-Gd** (C) under various pH conditions at 25 °C. The circle and square symbols represent r_1 and r_2, respectively. The concentration of Gd is presented in mM.

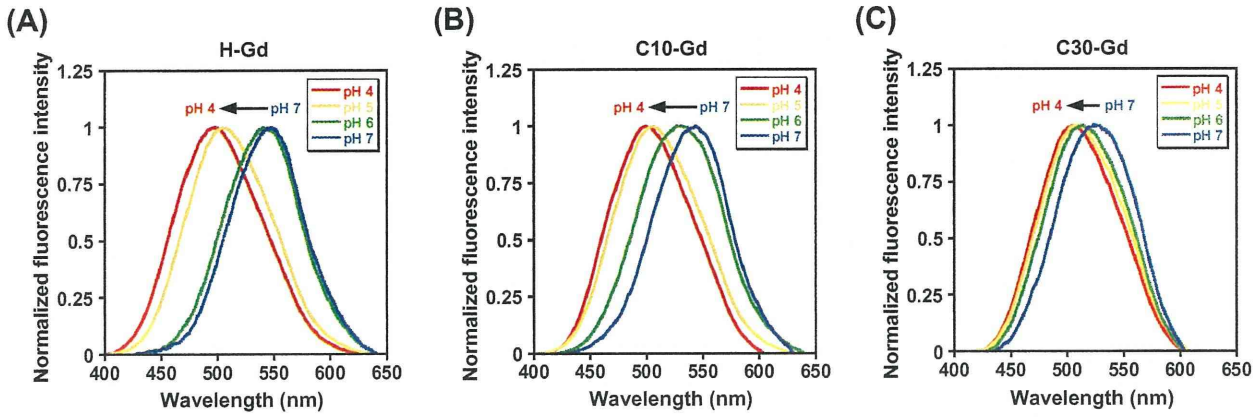

Figure 5. Fluorescence spectra of **H-Gd** (A), **C10-Gd** (B), and **C30-Gd** (C) at 25 °C. λ_{ex} = 330 nm. Red, yellow, green, and blue lines represent pH 4, 5, 6, and 7, respectively.

Table 2
Fluorescence decay parameters of **H-Gd**, **C10-Gd**, and **C30-Gd** under various pH conditions

pH	H-Gd		C10-Gd		C30-Gd	
	τ_1, τ_2 (ns)	F_1, F_2[a] (%)	τ_1, τ_2 (ns)	F_1, F_2[a] (%)	τ_1, τ_2 (ns)	F_1, F_2[a] (%)
4	5.7, 21.7	16, 84	7.1, 20.4	19, 81	7.8, 19.9	22, 78
5	6.7, 21.4	19, 81	7.2, 20.8	23, 77	7.2, 20.0	23, 77
6	3.4, 11.2	86, 14	4.7, 17.0	67, 33	6.3, 19.0	34, 66
7	2.7, 6.3	85, 15	3.5, 11.4	89, 11	5.4, 16.5	56, 44

[a] Fraction (F_i) of τ_i was defined as $100 \times I_i/(I_1 + I_2)$, ($i$ = 1, 2); I_i is the pre-exponential factor (please see Section 4).

attached to a linear polymer. However, the fluorescence decay parameters of **C30-Gd** were found to be quite different from those of **H-Gd** and **C10-Gd**. In **C30-Gd**, the long-lifetime component (τ_2) was almost constant at a pH between 4 and 7, and the pH-responsive change in the fraction of τ_2 was much smaller than that of **H-Gd** and **C10-Gd**. This is most likely due to the rigid structure of **C30-Gd,** which results from the high degree of cross-linking, making the surrounding environment of dansyl groups less susceptible to changes in pH. These results were consistent with the results from DLS and fluorescence spectra.

Fluorescence lifetimes (τ_F) were calculated as weighted average values based on τ_1 and τ_2 (please see the Section 4). Calculated τ_F was shown to increase with decreasing pH (Fig. 6), and the τ_F of **H-Gd** and **C10-Gd** significantly changed between pH 5 and 6.

2.3. Elucidation of the molecular switch mechanism

2.3.1. Fluorescence anisotropy measurements

The fluorescence anisotropy provides information about the molecular motion, in that it increases as the molecular motion of the fluorophores becomes slower. Thus, we measured the fluorescence anisotropies of **H-Gd**, **C10-Gd**, and **C30-Gd** at the wavelength of their emission maximum at each pH (Fig. 7), which showed that the molecular motion of all polymers became slower with a decreasing pH. Moreover, as the cross-linking degree increased, the molecular motion was restricted. These results agreed with our initial hypothesis that the pH-response of the relaxivity is because of the alteration of the molecular motion.

2.3.2. Calculation of rotational correlation time

It is known that rotational correlation time (τ_R) is one of the factors that affect the relaxivity of the CA, and provides quantitative information about the molecular tumbling.[1,23] Therefore, estimating behaviors of τ_R could be significantly helpful in designing and

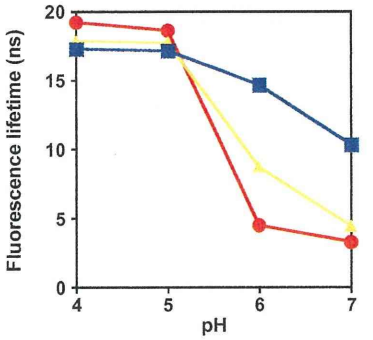

Figure 6. Fluorescence lifetimes of **H-Gd** (circle symbol), **C10-Gd** (triangle symbol), and **C30-Gd** (square symbol) at 25 °C. λ_{ex} = 370 nm. λ_{em} is in the range of 498–548 nm.

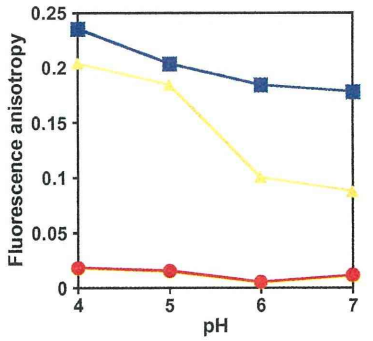

Figure 7. Fluorescence anisotropies of **H-Gd** (circle symbol), **C10-Gd** (triangle symbol), and **C30-Gd** (square symbol) at 25 °C. λ_{ex} = 330 nm. λ_{em} is in the range of 498–548 nm.

developing switchable CAs. The τ_R can be calculated from Perrin-Weber Eq. 1.[21,24]

$$A_0/A = 1 + \tau_F/\tau_R \quad (1)$$

In Eq. 1, A and τ_F represent the fluorescence anisotropy and fluorescence lifetime, respectively. A_0 is the limiting fluorescence anisotropy when no rotational diffusion occurs. The A_0 of dansyl fluorophores was experimentally determined to be 0.325 by Hu et al.[25]

The τ_R was calculated using measured values of A and τ_F (Fig. 8 and Supplementary Table S1–3), and the pH-response of τ_R was

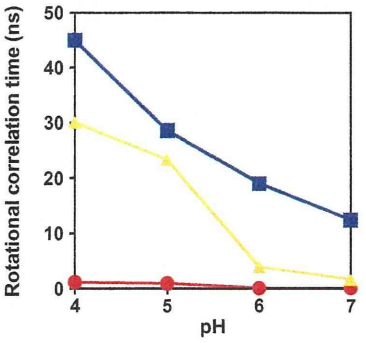

Figure 8. Rotational correlation times of **H-Gd** (circle symbol), **C10-Gd** (triangle symbol), and **C30-Gd** (square symbol) at 25 °C.

shown to be highly correlated with that of relaxivity. This result indicates that pH-responsive τ_R alterations caused changes in the relaxivities. Moreover, τ_R values of cross-linked **C10-Gd** and **C30-Gd** were much higher than those of **H-Gd**. Thus, it was expected that the relaxivity enhancement of cross-linked polymers was result of the increase of τ_R values. The linear structure is assumed to be a two-dimensional structure. As a result, the side chains can move relatively freely from the polymer backbone. In contrast, the cross-linked spherical shape is a three-dimensional structure, the inside of which is like highly wired polymer network. This network restricts the free movement of the side chains and extends the τ_R values.

Although **C30-Gd** expressed the small morphological change at low pH (Fig. 3 and Fig. 5), the relaxivities drastically increased at the pH region. Since the τ_R values of **C30-Gd** significantly increased at low pH (Fig. 8), it is expected that 30% of the cross-linking little restricts the pH-response in the local molecular tumbling, but it highly restricts that in the entire morphology.

The τ_R of **H-Gd** were below 1.1 ns and significant smaller than previous results obtained from a linear polymer with hydrophobic octyl groups, the maximum τ_R value of which is 12.8 ns at pH 4.[10] Nevertheless, the relaxivity values of **H-Gd** were maintained close to those of previous one. It is likely that the absence of hydrophobic groups and the difference of buffer conditions caused high relaxivities of **H-Gd** despite its fast molecular tumbling.

In summary, fluorescence studies and following calculation of τ_R values indicated that pH-responsive morphological changes in **H-Gd**, **C10-Gd**, and **C30-Gd** altered the rotational motion of their side chains, and caused their relaxivity switch properties. These results also demonstrated that spherical cross-linked polymers have more significant applicability to the design of switchable CAs, because increase of the cross-linking degree induced the relaxivity enhancement by restricting the molecular tumbling while maintaining the switching property (Fig. 9).

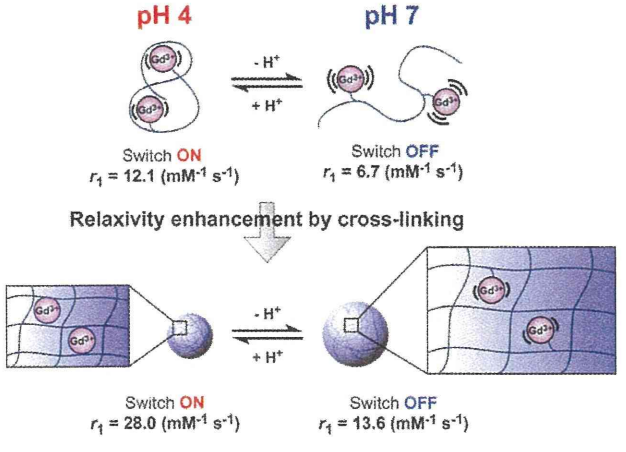

Figure 9. Proposed principle of molecular switches of **H-Gd** and **C30-Gd**.

3. Conclusions

Here, we applied morphological changes of pH-responsive polymers as a novel molecular switching process for MRI. The pH-responsive CAs were developed by attaching Gd^{3+} complexes and dansyl fluorophores to a linear homopolymer or spherical polymers. The relaxivities of the all polymers increased with a decreasing pH. The fluorescence studies indicated that the relaxivity change of the polymers is due to the alteration of the molecular correlation time τ_R caused by the pH-responsive morphological changes. A higher degree of cross-linking enhanced the relaxivities while maintaining the switching response; therefore, the cross-linked spherical polymers were found to be promising materials for the development of switchable CAs. Since such intelligent behaviors of spherical polymers have recently attracted much attention in the field of drug delivery,[11,26] our novel approaches also could lead to valuable biomedical applications in combination with drug delivery systems.

4. Experimental section

4.1. General procedures

The chemicals used in these experiments were obtained from Tokyo Chemical Industries, Wako Pure Chemical, and Aldrich Chemical Company. Because all the materials were purchased at the highest grade available, they were used without further purification. NMR spectra were recorded on a JEOL JNM-AL400 instrument at 400 MHz for ^1H and at 100.4 MHz for ^{13}C with tetramethylsilane as an internal standard. ESI-TOF MS were taken on a Waters LCT-Premier XE. Relaxation times were measured on a Bruker Optics minispec mq20. The inversion-recovery sequence and Carr–Purcell–Meiboom–Gill sequence were used for the measurements of T_1 and T_2, respectively. The r_1 and r_2 were respectively determined from the slopes obtained by plotting at least four points of $1/T_1$ and $1/T_2$ versus the concentration of the CA. Fluorescence spectra and fluorescence anisotropy were measured using a Hitachi F4500 spectrometer. Fluorescence decays were measured using a Horiba TemPro. DLS was performed using a Horiba SZ-100. TEM was performed using a Hitachi H-800 operated at 200 kV. ICP-MS were taken on an Agilent Technologies 7500cs.

Twice-diluted McIlvaine buffers (pH 4–7) were used as solutions for the pH adjustment and were prepared by mixing an arbitrary amount of 0.1 M citric acid aqueous solution with a 0.2 M disodium hydrogen phosphate aqueous solution.

4.2. Synthesis

4.2.1. PMAA, C10, and C30

Polymers were synthesized by distillation precipitation polymerization with a slight alteration, as follows.[17] For the synthesis of C10, 598 mg (6.95 mmol) of MAA, 32 mg (0.21 mmol) of MBAAm cross-linker (5 wt % of total monomer and cross-linker), and 13 mg (0.079 mmol) of 2,2′-azobisisobutyronitrile (AIBN) initiator (2 wt % of total monomer and cross-linker) were dissolved in 80 mL of acetonitrile in a dried two-neck flask fitted with a fractionating column, a condenser, and a receiving flask. The mixture was kept under an argon atmosphere and heated from room temperature

to boiling state within 15 min. Polymerization was performed until approximately 40 mL of acetonitrile was distilled from the reaction system within 60 min. The product was then purified three times by the following processes: centrifugation, decantation, and resuspension in acetonitrile with ultrasonication. The purified product was dissolved in distilled water and filtered through a Millipore 0.8 μm filter. The filtrate was freeze-dried, and a white powder was obtained. C30 was synthesized by altering the amount of MBAAm to 20 wt % of the combined weight of monomer and cross-linker. In the case of PMAA, no cross-linker was added to the reaction mixture. The amounts of total monomer and cross-linker were maintained at 1 wt % relative to the reaction medium, and the amounts of AIBN were maintained at 2 wt % relative to the total monomer and cross-linker.

4.2.2. H-Gd, C10-Gd, and C30-Gd

For the synthesis of **H-Gd**, 100 mg of PMAA was dissolved in 20 mL of anhydrous *N*,*N*-dimethylformamide (DMF) in a three-neck flask and stirred under argon. 267 mg (1.39 mmol) of 1-ethyl-3-(3-dimethylaminopropyl)carbodiimide hydrochloride (WSCD·HCl), 188 mg (1.39 mmol) of 1-hydroxybenzotriazole (HOBt), and 180 mg (1.39 mmol) of *N*,*N*-diisopropylethylamine (DIEA) were added to the solution. The molar quantity of these reagents was maintained at 1.2 equiv of carboxyl groups of the polymer. After 30 min, 3.0 mg (0.0050 mmol, 2.5 wt % of the weight of the polymer) of Gd(AEDO3A) and 2.0 mg (0.0070 mmol, 2.0 wt % of the weight of the polymer) of dansyl ethylenediamine were added to the mixture, which was stirred overnight at room temperature. The DMF was then evaporated under reduced pressure, and a yellow oil was obtained. The residue was dissolved in 1.0 M NaOH aq and then neutralized by 1.0 M HCl aq. The solution was purified by ultrafiltration using a Sartorius VIVASPIN (MWCO 3000). The supernatant was freeze-dried, and a white powder was obtained.

The synthetic procedures for **C10-Gd** and **C30-Gd** were identical to that of **H-Gd,** but required a different purification process. After the evaporation of DMF, **C10-Gd** and **C30-Gd** were purified by performing the following processes five times: centrifugation, decantation, and resuspension in methanol with ultrasonication. The products were then dissolved in 1.0 M NaOH aq and neutralized by 1.0 M HCl aq. Next, the solutions were centrifuged and washed with distilled water several times. The purified products were freeze-dried, and white powders were obtained.

Gd(AEDO3A) and dansyl ethylenediamine were synthesized according to previous reports.[18,19]

4.3. Fluorescence lifetime measurements

The fluorescence decay curve of **H-Gd** was acquired and fitted to the double-exponential Eq. 2. In the case of **C10-Gd** and **C30-Gd**, fluorescence decay curves were fitted with triple-exponential components because of the light scattering light.

$$I(t) = I_1 exp(-t/\tau_1) + I_2 exp(-t/\tau_2) \quad (2)$$

The weighted average fluorescence lifetime (τ_F) was calculated using Eq. 3 by excluding the light scattering component. The lifetime of the scattering light was on the tens of picoseconds timescale, which is much shorter than the nanosecond timescale of the fluorescence lifetime.

$$\tau_F = \tau_1 I_1/(I_1 + I_2) + \tau_2 I_2/(I_1 + I_2) \quad (3)$$

Acknowledgments

This work was partially supported by the Japan Society for the Promotion of Science (JSPS) through its 'Funding Program for World-Leading Innovative R&D on Science and Technology (FIRST) Program' and by the Ministry of Education, Culture, Sports, Science, and Technology (MEXT) of Japan (Grant No. 20675004, 21685019, and 22108519). The Takeda Science Foundation, the Mochida Memorial Foundation, and the Naito Foundation also provided support. The Asahi Glass Foundation provided financial support. Part of the present experiments was carried out in a facility at the Research Center for Ultra-High Voltage Electron Microscopy at Osaka University. S.O. received support from the Global COE Program 'Global Education and Research Center for Bio-Environmental Chemistry' of Osaka University and the JSPS Fellowship for Young Scientists.

Supplementary data

Supplementary data associated with this article can be found, in the online version, at doi:10.1016/j.bmc.2011.12.005.

References and notes

1. Lauffer, R. B. *Chem. Rev.* **1987**, *87*, 901.
2. Jun, Y.-w.; Lee, J.-H.; Cheon, J. *Angew. Chem., Int. Ed.* **2008**, *47*, 5122.
3. Louie, A. Y.; Hüber, M. M.; Ahrens, E. T.; Rothbächer, U.; Moats, R.; Jacobs, R. E.; Fraser, S. E.; Meade, T. J. *Nat. Biotechnol.* **2000**, *18*, 321.
4. Hanaoka, K.; Kikuchi, K.; Terai, T.; Komatsu, T.; Nagano, T. *Chem. Eur. J.* **2008**, *14*, 987.
5. Zhang, X.-A.; Lovejoy, K. S.; Jasanoff, A.; Lippard, S. J. *Proc. Natl. Acad. Sci. U.S.A.* **2007**, *104*, 10780.
6. Que, E. L.; Gianolio, E.; Baker, S. L.; Wong, A. P.; Aime, S.; Chang, C. J. *J. Am. Chem. Soc.* **2009**, *131*, 8527.
7. Zhang, S.; Wu, K.; Sherry, A. D. *Angew. Chem., Int. Ed.* **1999**, *38*, 3192.
8. Tóth, É.; Bolskar, R. D.; Borel, A.; González, G.; Helm, L.; Merbach, A. E.; Sitharaman, B.; Wilson, L. J. *J. Am. Chem. Soc.* **2005**, *127*, 799.
9. Aime, S.; Fedeli, F.; Sanino, A.; Terreno, E. *J. Am. Chem. Soc.* **2006**, *128*, 11326.
10. Okada, S.; Mizukami, S.; Kikuchi, K. *ChemBioChem* **2010**, *11*, 785.
11. Hu, Y.; Litwin, T.; Nagaraja, A. R.; Kwong, B.; Katz, J.; Watson, N.; Irvine, D. J. *Nano Lett.* **2007**, *7*, 3056.
12. Yang, X.; Chen, L.; Huang, B.; Bai, F.; Yang, X. *Polymer* **2009**, *50*, 3556.
13. Gota, C.; Okabe, K.; Funatsu, T.; Harada, Y.; Uchiyama, S. *J. Am. Chem. Soc.* **2009**, *131*, 2766.
14. Tanaka, K.; Kitamura, N.; Chujo, Y. *Macromolecules* **2010**, *43*, 6180.
15. Hoshino, Y.; Koide, H.; Urakami, T.; Kanazawa, H.; Kodama, T.; Oku, N.; Shea, K. J. *J. Am. Chem. Soc.* **2010**, *132*, 6644.
16. Oda, Y.; Kanaoka, S.; Sato, T.; Aoshima, S.; Kuroda, K. *Biomacromolecules* **2011**, *12*, 3581.
17. Liu, G.; Yang, X.; Wang, Y. *Polym. Int.* **2007**, *56*, 905.
18. Li, C.; Li, Y.-X.; Law, G.-L.; Man, K.; Wong, W.-T.; Lei, H. *Bioconjugate Chem.* **2006**, *17*, 571.
19. Shea, K. J.; Stoddard, G. J.; Shavelle, D. M.; Wakui, F.; Choate, R. M. *Macromolecules* **1990**, *23*, 4497.
20. Hu, Y.; Smith, G. L.; Richardson, M. F.; McCormick, C. L. *Macromolecules* **1997**, *30*, 3526.
21. Hu, Y.; Armentrout, R. S.; McCormick, C. L. *Macromolecules* **1997**, *30*, 3538.
22. Li, Y.-H.; Chan, L.-M.; Tyer, L.; Moody, R. T.; Himel, C. M.; Hercules, D. M. *J. Am. Chem. Soc.* **1975**, *97*, 3118.
23. Caravan, P. *Chem. Soc. Rev.* **2006**, *35*, 512.
24. Weber, G. *Biochem. J.* **1952**, *51*, 145.
25. Hu, Y.; Horie, K.; Ushiki, H. *Macromolecules* **1992**, *25*, 6040.
26. Oishi, M.; Hayashi, H.; Iijima, M.; Nagasaki, Y. *J. Mater. Chem.* **2007**, *17*, 3720.

DOI: 10.1002/asia.201100647

Fluorogenic Protein Labeling through Photoinduced Electron Transfer-Based BL-Tag Technology

Kalyan K. Sadhu,[a] Shin Mizukami,[a, b] Carolyn R. Lanam,[a] and Kazuya Kikuchi*[a, b]

In recent years, protein labeling has been routinely performed with various fluorescent markers.[1] The labeling of proteins allows monitoring of the specific location, movement, and interaction of proteins with other intracellular components using fluorescence microscopy.[2] For several decades, the labeling strategy mostly dealt with green fluorescent protein (GFP) and its variants. In order to overcome the unaltered fluorescent property and uncontrolled expression time of GFP, small molecular probe-based labeling approaches for live-cell imaging methods have been developed.[3] However, most of the reported small-molecule labeling probes do not show different fluorescence properties for the labeled and unlabeled states. Fluorescein-based arsenical hairpin binder (FlAsH) and resorufin-based arsenical hairpin binder (ReAsH) are the pioneer techniques for fluorogenic protein labeling with small molecular probes.[4]

In our earlier studies, we developed a site-specific protein labeling technique that employs a genetically modified β-lactamase (BL-tag).[5] Mutation at a specific position in TEM-1 (class A β-lactamases) provides turn-on fluorogenic biosensors involving a β-lactam ring. The reaction of wild-type TEM-1 (WT TEM) with the β-lactam moiety involves acylation and deacylation steps.[6] We have utilized the BL-tag protein for covalent attachment with a substrate. Despite the similar molecular weights of the BL-tag and GFP, fluorogenicity can be introduced only through the BL-tag technology.

We have developed a fluorogenic mechanism based on aggregation–elimination processes for highly selective protein labeling with a fluorophore of desired color using the BL-tag technology. We have also shown a broad applicability of dinitrobenzene (DNB) as a quencher.[5c,d] However, the limitation of the technology is a slow fluorogenic response of the synthesized probes such as **CCDNB**, which carries a coumarin fluorophore moiety, a cephalosporin moiety, and DNB (Figure 1). The necessary incubation time for a cell imaging experiment using **CCDNB** was 60 minutes. To reduce the incubation time for the imaging experiments, we aimed at developing more sophisticated probes that possess the DNB quencher. Herein, we report two newly designed probes with shorter linkers compared to those of **CCDNB**. In addition, we modified slightly the quencher in one probe. The probe with the modified quencher showed a comparatively fast fluorogenicity in vitro and in live-cell imaging studies. Fluorescence lifetime measurements indicated a different quenching mechanism for the most active probe. A detailed analysis of this new fluorogenic mechanism revealed a photoinduced electron transfer (PET) process[7] from the fluorophore donor to the quencher acceptor.

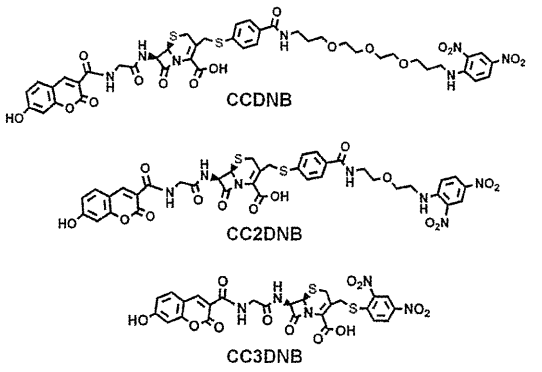

Figure 1. Chemical structures of the synthesized fluorescent probes used for protein labeling.

The two new probes **CC2DNB** and **CC3DNB** that have a comparatively short or no linker between the β-lactam and quencher, respectively, are depicted in Figure 1. 2-(2-Aminoethoxy)ethanamine was used as the linker between the cephalosporin part and the DNB quencher in **CC2DNB**. A coumarin derivative was attached to the opposite side of cephalosporin through a glycine linker to synthesize the **CC2DNB** probe. On the other hand, the synthesis of **CC3DNB** did not require any linker between the cephalosporin part and the quencher. 2,4-Dinitrothiophenol was directly introduced as a quencher to the cephalosporin part to synthesize **CC3DNB**.

[a] Dr. K. K. Sadhu, Dr. S. Mizukami, C. R. Lanam, Prof. Dr. K. Kikuchi
Division of Advanced Science and Biotechnology
Graduate School of Engineering
Osaka University
2-1 Yamadaoka, Suita, Osaka 565-0871 (Japan)
Fax: (+81) 6-6879-7875
E-mail: kkikuchi@mls.eng.osaka-u.ac.jp

[b] Dr. S. Mizukami, Prof. Dr. K. Kikuchi
Immunology Frontier Research Center
Osaka University
3-1 Yamadaoka, Suita, Osaka 565-0871 (Japan)

Supporting information for this article is available on the WWW under http://dx.doi.org/10.1002/asia.201100647.

Absorption spectra of **CC2DNB** and **CC3DNB** were recorded in 100 mM HEPES buffer (pH 7.4, Figure 2a) and methanol (Figure 2b), and compared with those of **CCDNB** under similar conditions. The reported absorption maxima of 348 nm for free *N*-ethyl-substituted 2,4-dinitroaniline[8]

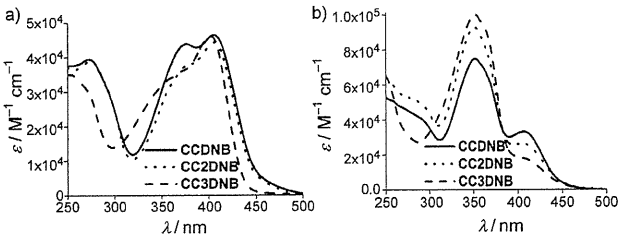

Figure 2. Absorbance spectra of **CCDNB**, **CC2DNB**, and **CC3DNB**. a) Spectra in 100 mM HEPES buffer (pH 7.4). b) Spectra in methanol.

and of 362 nm for 1-(methylthio)-2,4-dinitrobenzene[9] in methanol are quite similar to the observed absorption peaks at 350 nm in methanol for the synthesized probes containing the DNB part. In aqueous buffer, the absorption maxima for the coumarin and DNB parts of both **CCDNB** and **CC2DNB** were observed at 407 nm and 375 nm, respectively. Under the same conditions, the corresponding absorption peaks in **CC3DNB** were detected at 402 nm and 356 nm (shoulder band), respectively. The observed shift of the latter peak was due to the different DNB linkage in this probe. The slight blue shift in the absorption peak of coumarin in **CC3DNB** suggested a change in the interaction between the coumarin and DNB parts within this probe. Comparative measurements with the previously reported probe **CA**[5b] (Figures S3 and S4 in the Supporting Information) confirmed that the peaks around 356 nm or 375 nm in the new probes were due to the quencher DNB parts.

Next, we measured the fluorescence emission spectra of the free probes in 100 mM HEPES buffer of pH 7.4 (physiological pH) and compared them with those in methanol[10] (Figure S5 in the Supporting Information). The fluorescence signals of all the probes were sufficiently quenched in the aqueous buffer (Table 1). The strength of the interaction between the fluorophore and the quencher was comparable for **CCDNB** and **CC2DNB** due to the similar nature of the interacting parts. However, maximum fluorescence quenching was observed in the case of **CC3DNB**. The measured emission spectrum of **CA** in aqueous buffer (Figure S4 in the Supporting Information) confirmed the quenched state of the fluorophore in the newly synthesized probes.

Table 1. Fluorescence quantum yields of the synthesized probes in buffer of physiological pH and in methanol.

Solvent	Fluorescence quantum yield (Φ)		
	CCDNB[5d]	**CC2DNB**	**CC3DNB**
100 mM HEPES buffer (pH 7.4)	0.04	0.04	0.02
Methanol	0.19	0.19	0.19

The fluorogenicities of the synthesized probes were studied by measuring the enhancement of the fluorescence intensity of each probe in the presence of the BL-tag and WT TEM. The reaction rates in the presence of WT TEM were faster for all three probes as compared to the rates in the presence of the BL-tag (Figure 3). In our earlier study, we found that the quencher part was eliminated from the **CCDNB** probe in the presence of the BL-tag.[5d] To modulate the elimination kinetics, the **CC2DNB** probe was synthesized with a much shorter linker compared to the previous polyethylene glycol spacer. However, there was only a slight enhancement in the reaction rate in the presence of the BL-tag. The rate of fluorescence enhancement with the BL-tag was the fastest for **CC3DNB** (Figure 3).

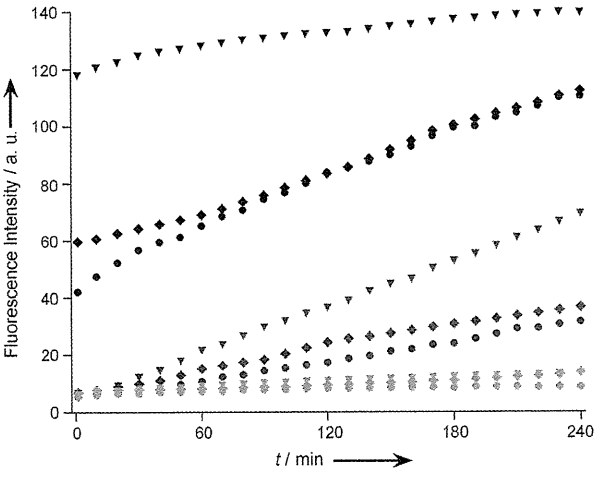

Figure 3. Change in the fluorescence intensities of **CCDNB**, **CC2DNB**, and **CC3DNB** (1 μM each) with time in the presence of WT TEM or BL-tag (0.5 μM each) in 100 mM HEPES buffer (pH 7.4) containing 0.1% DMSO at 25°C. Marker and color codes, circles: **CCDNB**, squares: **CC2DNB**, triangles: **CC3DNB**; black: WT TEM, dark grey: BL-tag, light grey: free probe.

The difference in the rates of fluorescence enhancement indicates that the removal of the quencher in **CC3DNB** is faster compared to the removal of the quencher in the other quenched probes. The overall stability of the eliminating groups partly controls the removal of quenchers from the probes. In the case of **CC3DNB**, the eliminating thiophenolate anion is sufficiently stabilized due to the presence of two highly electron-withdrawing nitro groups at the 2- and 4-positions. On the other hand, such stabilization was less pronounced in the **CCDNB** and **CC2DNB** probes owing to the less electron-withdrawing monosubstituted amide functional group at the 4-position of the thiophenol parts (Figure S6 in the Supporting Information).

The fluorescence enhancements of the different probes were not the same, even in the presence of WT TEM. Approximately 36% and 45% of the reactions were completed within 1 minute during the incubation of WT TEM with **CCDNB**[5d] and **CC2DNB**, respectively. The highest rate of

